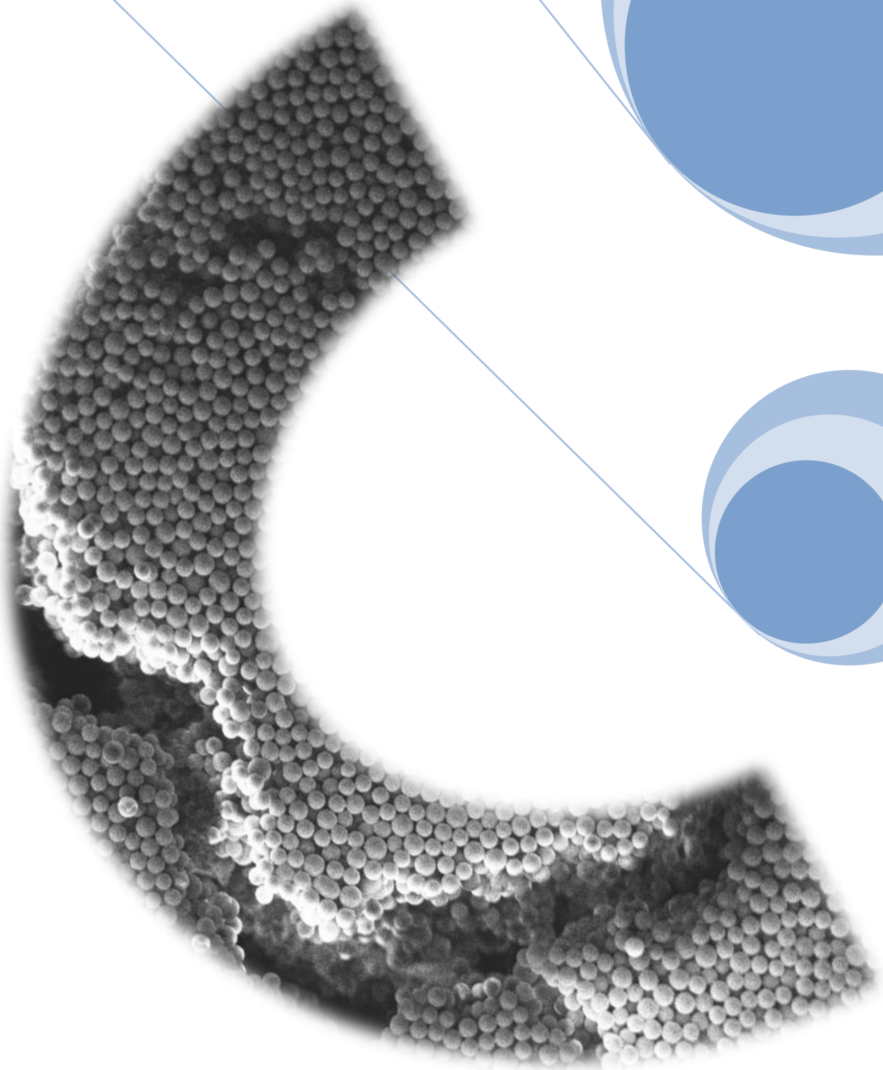

Synthesis and Filtration Dewatering of Model Colloids in the μm Range

Master Dissertation at Aalborg University

Søren Lorenzen

31/5/2012

Preface

This work is based upon studies done at the 9th and 10th semester of the Master of Science in Chemistry education. The studies were carried out at the Section of Chemistry, Department of Biotechnology, Chemistry and Environmental Engineering at Aalborg University.

A list of abbreviations and symbols used throughout this work can be found in Appendix A, while a list of all the chemicals used can be found in Appendix B.

Citations are made as numerical references, which will apply to the entire paragraph if placed after a full stop, but only to the previous sentence if placed before the full stop. The bibliography is found in Appendix D, sorted by the numbers given, to the sources, in the text.

I would like to thank Jens Rafaelsen at the department of Physics and Nanotechnology for taking the SEM-pictures used in this work and my fellow students for taking part in various discussions. Special thanks go to my wife, Annemette and my three daughters for their patience and good spirit.

Aalborg, 31-05-2012

Søren Lorenzen

Table of Contents

Dansk resume (Danish abstract)

Når en membran filtrerings proces skal anvendes, er en forudgående model af interaktionerne, mellem de suspenderede stoffer og membranen, ofte krævet. De fleste af de matematiske modeller, der anvendes i dag, stammer fra eksperimenter baseret på uorganiske partikler og er ofte utilstrækkelige til beskrive komplekse systemer, såsom spildevand af forskellig oprindelse, som ofte er både kompresibel og negativt ladet. For at forbedre disse modeller, skal der bl.a. bruges organiske partikler, med kontrollerbar egenskaber.

Denne rapport undersøger dispersions polymerisering af methylmethacrylat med polyvinyl-pyrrolidone som stabilisator, samt styren med poly(acrylic acid), som en mulig metode til at fremstille partikler med de nævnte egenskaber.

I den første del af rapporten beskrives den anvendte dispersion polymeriseringen og er en kombination af litteratur studier og eksperimentelt arbejde. Den anden del er stempel filtrering af de fremstillede partikler og er sammensat af en beskrivelse af de matematiske modeller der anvendes i dag til at forudsige den specifikke filtreringsmodstand, α, efterfulgt af resultaterne fra filtreringseksperimenterne.

Der er fundet ud af, at værdierne for α, når partikler fremstillet fra methylmethacrylat og polyvinylpyrrolidon filtreres, er tæt på den modelerede værdi, mens α er betydeligt højere for partikler fremstillet fra styren og poly(acrylic acid). Dette skyldes sandsynligvis de interaktioner, som finder sted mellem partiklernes ladede overflade og vandet.

Udover dette viste kun én af partiklerne, en lille trykafhængighed af α og kun når der blev filtreret over længere tid (større volumener). Dette skyldes formodentlig tilføjelsen af en overfladeaktiv monomer under syntesen, hvilket muligvis kan skabe et højere osmotisk tryk omkring partiklen.

Når mindre og større partikler blev blandet, blev modstanden hovedsageligt udgjort af de mindre partikler, sandsynligvis fordi de mindre partikler udfylder hulrummene mellem de større.

English abstract

When a membrane filtration process is to be used, a preceding model of the interactions between the suspended solids and the membrane is often required. Most of the mathematical models used today, stem from experiments using inorganic particles and are often inadequate in describing complex systems, such as municipal and industrial waste water. Filter cakes composed of such organic solids are often both compressible and negatively charged. To improve these models, organic particles with controllable properties, are in need.

This work investigates the dispersion polymerization, of methyl methacrylate with polyvinylpyrrolidone as stabilizer, as well as styrene with poly(acrylic acid), as a possible method to produce particles with the wanted properties.

The first part of this work describes the dispersion polymerization employed and is a combination of literature studies and experimental work. The second part is dead end dewatering filtration of the produced particles and are composed of a description of the mathematical models used today, to predict the specific resistance to filtration, α, followed by the results from the filtration experiments.

It was found that the values of α, when filtering particles made from methyl methacrylate and polyvinylpyrrolidone, are quite close to the predicted value, whereas α is significantly higher for the particles produced from styrene and poly(acrylic acid), probably due to the interactions taking place between the charged surface of the particles and the surrounding water.

In addition to this, only one of the particles showed a slight pressure dependency of α and only at longer filtration times (larger volumes). This is possibly caused by the addition of surface active monomer during the synthesis, which might create a higher osmotic pressure around the particle.

When smaller and larger particles were mixed, the resistance was shown to mainly be governed by the smaller particles, probably due to blinding effects, where the smaller particles fill the voids between the larger.

1 Introduction

Separation of solids and liquids are a process applied in a large variety of industrial fields and in a variety of forms, ranging from simple air drying to more advanced membrane filtration. The latter is used extensively in especially the food and medico industries and increasingly in municipal waste water plants as MBR's. The solid materials separated are typical organic substances, with sizes ranging from a few nm to several µm and with a diversity ranging from a few components to very complex systems.

When regarding membrane filtration of active sludge from waste water treatment plants, micro filtration membranes, with a pore diameter ranging from 0.1 to 10 µm, is most commonly employed.(1) To keep cost down, it is important that the separation module is correctly sized, according to its intended use, and this will typically require some sort of mathematical model or a lab-scale test plant. Since these models are greatly dependant on the material you want to separate, and often only apply well to inorganic particles(2), characterization of the materials properties will probably be one of the first things to do.

The active sludge can consist of many different components. Here amongst flocs of bacteria, organic fibers and inorganic particles all held together by extracellular polymeric substances (EPS). EPS will typically consist of a mixture of proteins, polysaccharides, DNA and different organic acid, e.g. humic acid. Due to the acid and protein contents of the EPS, the flocs will be charged, with every charge being associated with a counter ion. These charges and their counter ions will generate an osmotic pressure, swelling the EPS with up to 98 % water. (2)

Upon filtration, these flocs will, along with other material, not part of the flocs, deposit on the membrane. This is a part of, what is called fouling and will increase the membrane resistance by, among other things, generating a gel or cake layer on the membrane surface. The cake layer can act as a second membrane with different porosity and can be more or less compressible.(3) Cake layers consisting of activated sludge have been shown to be very compressible (4), probably due to their soft or loose nature and the high amount of water swollen material. This will affect the relationship between the membrane pressure drop and the flux of permeate through the membrane in such a way, that they will no longer be proportional, once the critical flux has been obtained(3).

Activated sludge is however not suitable for model material as it is way too complex. Systems resembling activated sludge, with known species of bacteria and a controlled nutrient feed still prove unusable. The properties of the flocs will simply change over time, as it is still a living system. It is therefore of high importance that the model material is non-living. Furthermore it must have the correct size and (simple) shape and remain that way, also under storage of longer periods. The production of such model particles/colloids still remains a challenge. (2)

2 The aim of this work

This work is divided into two parts with the following aims.

1. Is it possible to synthesize organic polymeric particles which can fulfill the following requirements?
    a. Non-living
    b. Spherical with a relatively narrow size distribution
    c. Sizes above 1 µm
    d. Non-flocculating
    e. Density close to water
    f. Preferably negatively charged
    g. Ability to swell in water dependent on pH
    h. Relatively easy control of the charge density and the particle size

2. How will the dewatering filtration of these particles, either by themselves or combined with each other, be affected by, primarily, particle size and charge density?

3 Part one – Synthesis of organic polymeric particles

This part will focus on the synthesis and analysis of organic polymeric particles with the properties outlined in section 2

3.1 Heterogeneous polymerization in general

Different methods of heterogeneous polymerization exists, each whit their own possibilities and limitations. The covered size ranges of the different methods are illustrated in Fig. 3.1 (5)

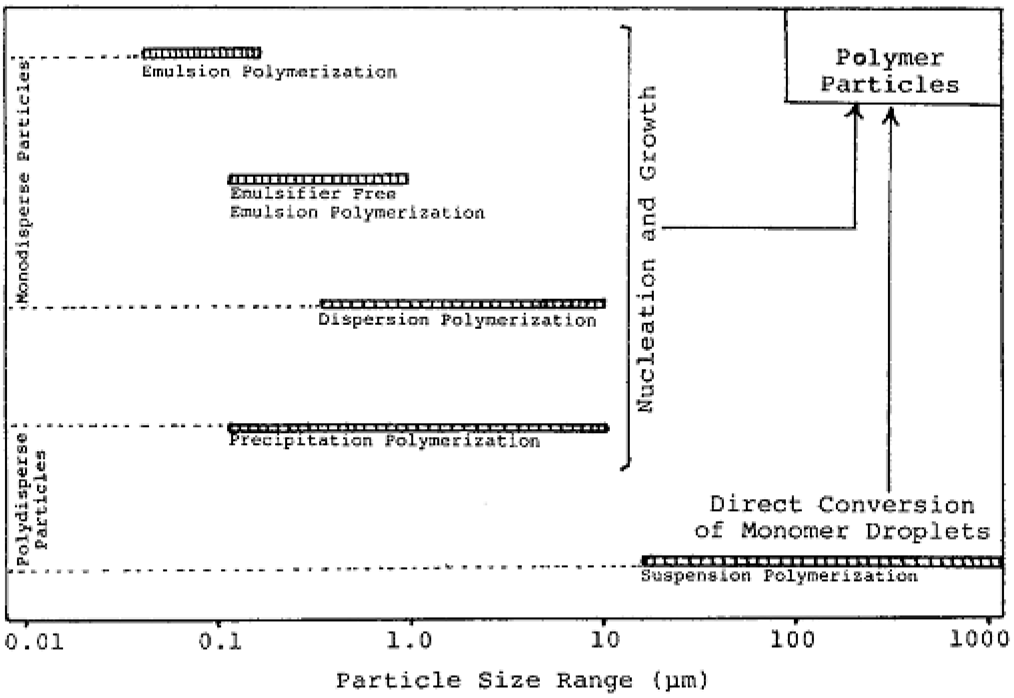

Fig. 3.1. Particle sizes obtained by 5 different heterogeneous polymerization techniques (5)

Precipitation and suspension polymerization both produces polydisperse particles(6) and has a poor control of particles size. The particle shape is often irregular, although suspension polymerization, in some instances, can produce spherical particles. Stabilization consists, in suspension polymerization mainly of loosely adsorbed steric stabilizers, such as high MW PEG's, whereas precipitation polymerization most often is unstabilized. (5)

Emulsion- and emulsifier-free emulsion polymerization of hydrophobic monomers in water, is probably the most common way of producing polymeric particles. This method results in monodisperse, spherical particles, between 50 and 1000 nm in diameter. The particles can be stabilized, either steric or electrostatic, by a multitude of different surfactants and, in the case of emulsifier-free emulsion polymerization, by a stabilizer produced *in situ*, by co-polymerization with a hydrophilic monomer, giving the particle a core/shell morphology, where the core and shell have different properties.(5),(7)

In the work of Hinge, et al., 2006, monodisperse polystyrene particles in the range of 200 to 500 nm with varying thickness of a polyacrylic acid shell have been synthesized by emulsifier-free emulsion polymerization and subsequently used for filtration experiments. By changing pH, the shell can be more or less swollen with water, but the core particle itself, consisting mainly of long chained polystyrene, can never swell with water.(8), (7) Dispersion polymerization can also produce monodisperse spherical particles, but the size range is typically between 0,5 and 10 µm. Since the solvent mostly consists of short chain alcohols or hydrocarbons, a larger catalogue of monomers, compared to emulsion polymerization, can be used.(5) Co-polymerization between monomers of different hydrophilicity can also, to some degree, be obtained with a more random distribution inside the particle, as opposed to the core/shell morphology obtained in emulsion polymerization (9). This opens up the possibility of producing particles which are swellable throughout the entire particle. The Stabilizers employed are most often steric, but electrostatic types have been used in some cases.(10) It has, furthermore, been shown that dispersion polymerization is effective in incorporating fluorescent molecules into the particles, making detektion by ultra violet radiation possible, if needed.(11)

Particles produced by dispersion polymerization, thus have the possibility of fulfilling all of the above mentioned criteria and have been the choice of method for this study.

3.2 Dispersion polymerization

Dispersion polymerization was originally developed using a hydrocarbon solvent and an oil soluble polymeric stabilizers more than 20 years ago. This was achieved in the search of an easy way of producing particles in between the size ranges of conventional emulsion polymerization and suspension polymerization. Later the concept was expanded to the use of polar solvents such as alcohols and much research has gone into the understanding of the particle formation and growth mechanisms and how to control and even predict/simulate the final particle size.(12)(10)

The following sections should give a basic understanding of how dispersion polymerization works.

3.2.1 Particle formation and growth

In dispersion polymerization, with the mechanism illustrated in Fig. 3.2, all of the starting materials, monomer, initiator and stabilizers are initially dissolved in the solvent.(5) (12)

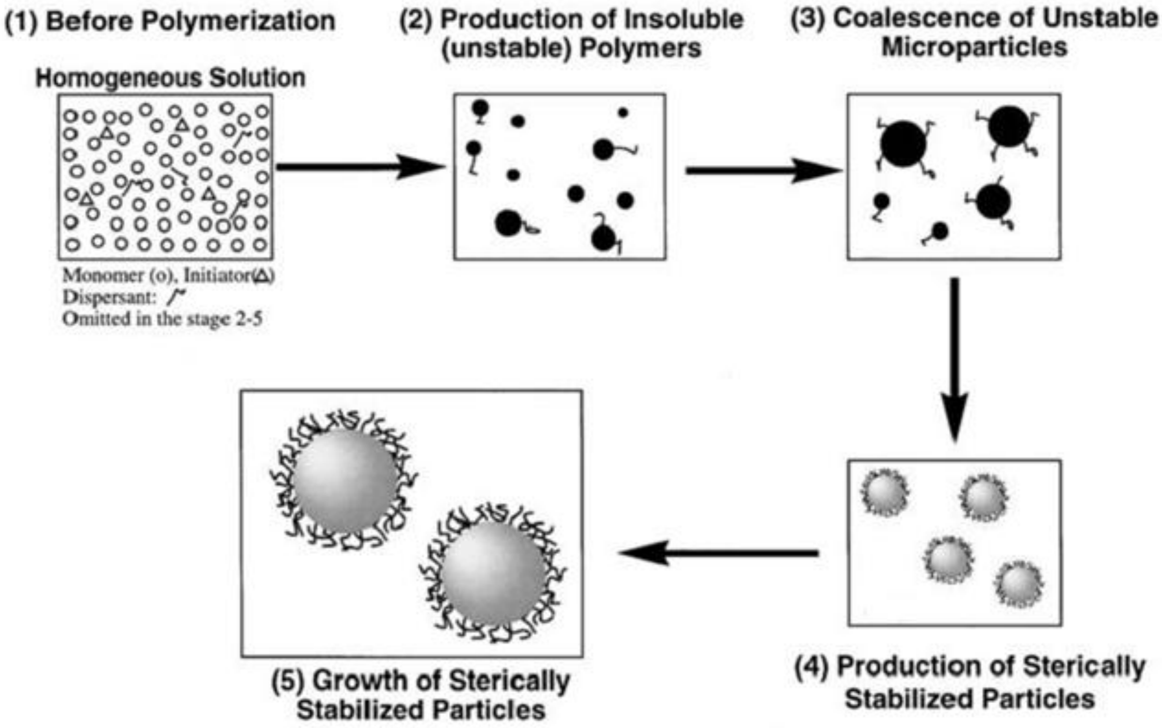

Fig. 3.2. Schematic representation of particle formation and growth in dispersion polymerization (10)

Polymerization is then initiated in this homogeneous mixture and the polymer chains will grow in solution, until a critical chain length is achieved. The polymers will then precipitate out and generate nuclei that, if large enough, will be stabilized by adsorption of stabilizer to the surface. If the nuclei are not large enough, or the available stabilizers are insufficient, the nuclei will coalesce until both requirements are fulfilled. Once stable, or mature, particles have formed, monomer will diffuse into- and swell the particles, allowing the propagation of the precipitated chains to continue inside the particles as bulk polymerization. (13), (14) Since solution polymerization still occurs throughout almost the entire reaction time, new oligomeric radicals and even new unstable nuclei from dead polymers can be formed, which might lead to the production of secondary particles. However, under favorable conditions, these products of solution polymerization will be scavenged by already existing larger particles.(15) This will continue until all monomer is used.

Simulations and experimental work carried out by others indicates that the particle count is fixed early in the reaction before 1 % conversion, and that it can take up to 20 times longer for the particles to achieve monodispersity. The reason for this is that particles of different sizes grow at different rates, since the adsorption of monomer and scavenging of oligomeric radicals and dead polymers from solution is governed by diffusion. This will allow the smaller particles to catch up in size, given enough time.(10)

3.2.2 Mechanism of stabilization

Stabilization is crucial in understanding the particle formation stage and it is generally accepted that this can happen in two different ways.

First there is the anchoring of a block or graft co-polymer, where one end of the polymer is highly soluble in the reaction medium, whereas the other end (the anchor) is not. This leaves the anchor more or less buried within the particles, while the soluble part protrudes out from the surface.(14) The block-type co-polymer is mostly of lower MW and the anchoring is somewhat reversible, making this type a typical co-stabilizer(13). The graft co-polymer is, on the other hand, typically produced *in situ,* by chain transfer of active radicals to a soluble polymer of higher MW, containing active α-hydrogens as possible chain transfer sites.

Chain transfer occurs when an active radical extracts a hydrogen atom, facilitating a homolytic cleavage of the bond between the α-carbon and the α-hydrogen. This produces an H-terminated compound (where the radical were before) and a new radical on the α-carbon. This new radical is, due to electron donating properties of the functional group, stable enough to propagate with monomer in solution.(16)

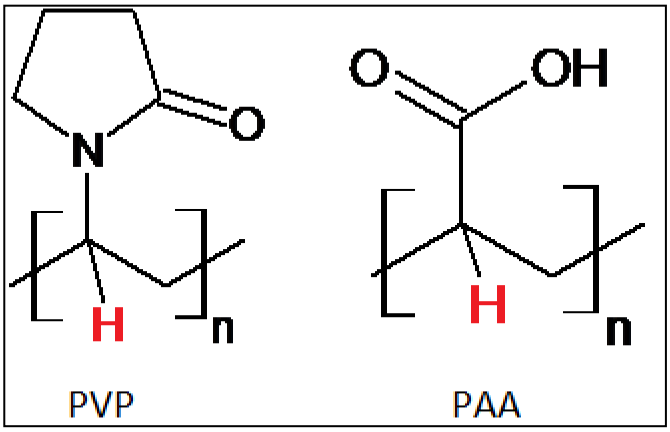

Fig. 3.3. PVP (left) and PAA (right) with the α-hydrogen highlighted in red

In polar solvents the, water and short-chain-alcohol soluble, polymer PVP (polyvinylpyrrolidone) is often used as a steric stabilizer, although many other polymers can be used. Among those, is PAA (polyacrylic acid) an interesting candidate, since it is a polyelectrolyte and stabilization thus is achieved by electrostatic forces instead of simply steric means. In Fig. 3.3 the α-hydrogen of

PVP and PAA is highlighted as a red **H**, while Fig. 3.4 is a schematic representation of the graft co-polymer in mention (proportions not to scale). The anchor part in the graft co-polymer is typically of much higher molecular weight than its counterpart from block co-polymers and is initially incorporated into the particle as an active radical chain end, which will propagate further inside the monomer swollen particle. This will make the anchor part covalently linked to the particle, making removal of the stabilizer from the particle highly unlikely.(14) The covalently linked stabilizers will behave as a "hairy" layer surrounding the particle(15), giving the particle some of the core/shell properties seen in emulsifier free emulsion co-polymerization of hydrophobic and hydrophilic monomers, as described earlier. The thickness of this layer depends on the MW of the stabilizer.

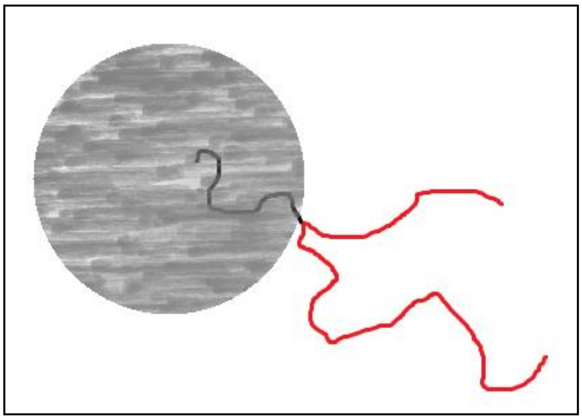

Fig. 3.4. Schematic representation of a particle (grey) with a graft co-polymer, where the anchor part (black) is buried inside the particle and the soluble part (red) is protruding from the surface

The second form of stabilization employed is the loose, and highly reversible, adsorption of soluble polymers to the particle surface. Some of the stabilizers used to make graft co-polymers are also believed to have some stabilizing effect by this method, and the two stabilization mechanisms are not necessarily mutually exclusive. (14) Other polymers, such as PEG's, will only act as an adsorbed steric stabilizer as they lack the active α-hydrogen.

3.2.3 Factors influencing particle size

Every single reaction parameter in dispersion polymerization is important when considering the size of the particles. Seemingly small changes can have great effect, as explained in the following. For simplicity, charts, examples and explanations will be given from a system of PVP stabilized PMMA particles in methanol with AIBN as initiator, unless otherwise stated.(17)

3.2.3.1 Reaction temperature

The temperature of the reaction will primarily affect the particle formation stage in the following ways. The viscosity of the medium will decrease, allowing a higher diffusion rate of nuclei/particles in the aggregation process. This will produce fewer but larger particles. The increase in diffusion rates will also make early termination of the PVP-g-PMMA more likely. The latter effect is enhanced even more by the increase in dissociation rate of the initiator into radical fragments, leading to the same effect as seen with increased initiator concentration.

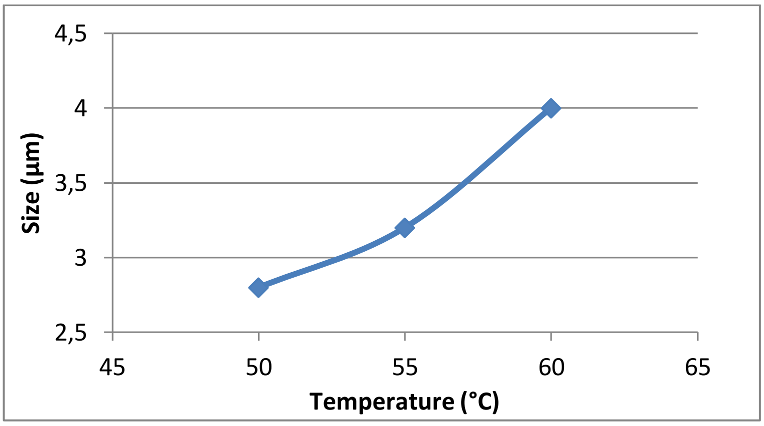

Fig. 3.5. Effect of reaction temperature on particle size. Data collected from Shen, et al., 1993

The solvency of the medium will also be affected by temperature in such a way, that the critical chain length before precipitation will increase, making the nuclei larger from the beginning, just as the solubility of PVP will increase making adsorption to the particle surface less likely, prolonging the aggregation time, again producing fewer but larger particles. If the temperature is too high, the aggregation phase will continue in the lack of sufficient stabilization, resulting in massive coagulation.(17) The combined effects on size can be seen in Fig. 3.5.

3.2.3.2 Initiator concentration

When the initiator concentration increases, particles size increase as well, as shown in Fig. 3.6. This can be explained by two processes involved in the particle formation stage. Firstly, the increased radical concentration will speed up the production of precipitated oligomeric radical chains, giving more material to aggregate. Secondly, the chance of early termination, of the stabilizer graft co-polymer, produces shorter anchor chains, increasing the solubility of the entire graft co-polymer, thus decreasing the adsorption rate.

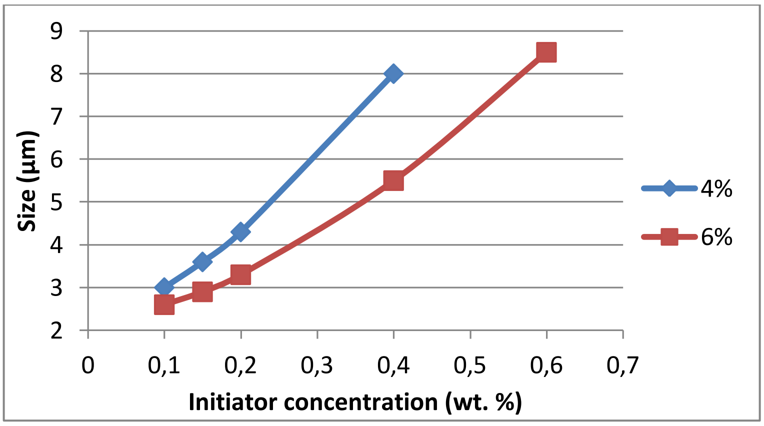

Fig. 3.6. Effect of AIBN concentrations on particle size at two different PVP-K30 (40 kDa) concentrations, keeping all other reaction parameters constant. Reproduced by data obtained from Shen, et al., 1993

Together this will prolong the aggregation process leading to larger, but fewer particles at the point where sufficient stabilization is obtained to produce mature particles. Because of the lower number density and thus a lower total surface area, the scavenging of new nuclei and dead polymers will be less likely. If the initiator concentration reaches a certain threshold, the scavenging will be so ineffective that new nuclei will be able to grow to mature particles themselves, resulting in an increase in particle size distribution. A similar effect has been observed for PS particles. (15) (17)

3.2.3.3 Concentration and molecular weight of stabilizer

The size dependency of the concentration and molecular weight of the stabilizer is a combination of changes in adsorption rates of stabilizer onto the particle surface (primarily concentration) and the viscosity of the medium. As expected, Fig. 3.7 shows the particle size to decrease with an increase in both concentration and molecular weight of PVP.(17)

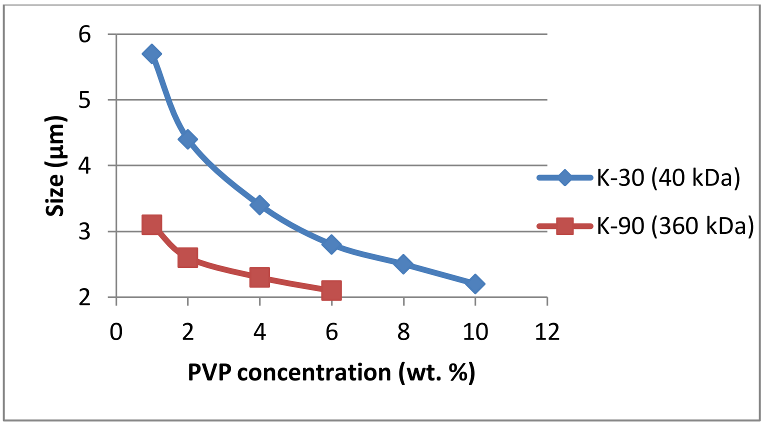

Fig. 3.7. Effect of concentration and molecular weight of PVP on particle size. Reproduced by data obtained from Shen, et al., 1993

This effect is however not considered to be universal amongst all combinations of monomer and stabilizer. In the work of Paine, et al., 1990, the styrene/PVP system behaves somewhat similar, but others have seen almost no dependency on concentration. It is however difficult to directly compare results from different experiments, as several other reaction parameters vary, especially the type, concentration or absence of a co-stabilizer.

3.2.3.4 Monomer concentration

Changing the initial monomer concentration will primarily affect the solvency of the medium, increasing the critical chain length with increasing monomer concentration.(15) Some systems have, however, shown an inverse tendency at the lower monomer concentration range. This is illustrated in Fig. 3.8 for a PMMA/PVP system.(17)

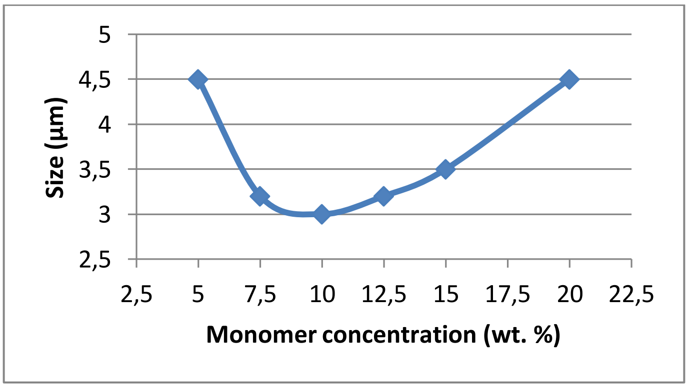

Fig. 3.8. Effect of initial monomer concentration on particle size. Reproduced by data obtained from Shen, et al., 1993

This phenomenon is thought to be caused by a competition between the change in solvency, as mentioned above, and a change in propagation rate of the polymer, which also has an impact on the length of the anchor part of PVP-g-PMMA. At low monomer concentrations the anchor is short and the stabilization less efficient, leading to larger particles.(17)

3.2.3.5 Solvent system

Dispersion polymerization can be carried out in many different solvent systems and solvency can affect particle size primarily by changing the critical chain length before precipitation of polymer and by changing the solubility of the stabilizer and/or grafted stabilizer. A mixture of water and methanol is commonly used for the preparation of smaller particles.(17)

3.3 Preparation of PVP stabilized PMMA particles

With the basics of dispersion polymerization and size control in mind a set of experiments were conducted. The aim of this was to investigate if the preparation of monodisperse PMMA particles with sizes above 6 µm is possible, and if the co-polymerization of MMA with MAA and NaMA would yield particles with charges embedded in the core.

Two sets of standard recipes were made, one with NaMA, called PMMA-A, and one with MAA, called PMMA-B. The ingredients used can be found in Table 3.1. The MAA was passed through a short column of activated aluminum oxide to remove the hydroquinone inhibitor. All other chemicals were used as received.

PMMA-A and PMMA-B	
Ingredient	Weight (g)
MMA	15
MAA/NaMA	0,375
PVP (65 kDa)	4
AIBN	0,2
MeOH	80,5

Table 3.1. List of ingredients in the standard recipes

In the first batch, MMA, NaMA, PVP and most of the MeOH was mixed, at room temperature, in a 250 mL two-necked round bottomed flask, purged with nitrogen for 15 minutes and heated to 60 °C. Then AIBN was dissolved, at room temperature, in the remaining MeOH (approx. 6 mL), purged with nitrogen for 15 min and added to the already heated mixture.

This procedure was, due to lack of workspace, however not possible for the batch containing MAA. Here all ingredients were mixed at once and then subsequently heated to reaction temperature.

The mixtures were allowed to react under nitrogen for 48 hours, before being cooled on ice, under normal atmosphere. The particles were cleaned by a repeating sedimentation/ redispersion process in methanol and stored in sealed PP-containers. The cleaning process will apply to all particles produced throughout this work, although some batches were stored in sealed glass bottles instead of PP-containers.

Several attempts to produce particles under more extreme conditions, such as less stabilizer, more initiator, higher temperature and combinations of these, were conducted, with all but one, called PMMA-C, ending in massive coagulation. Although some coagulation did also form in this, it was possible to separate the particles and clean them as described above. The ingredients can be found in Table 3.1, with the setup and temperature being the same as with the standard recipes.

PMMA-C	
Ingredient	Weight (g)
MMA	20
MAA/NaMA	0,5
PVP (65 kDa)	6
AIBN	0,6
MeOH	73

Table 3.2. List of ingredients in the one successful batch under more extreme conditions

Here the concentration of monomer, co-monomer and AIBN is increased which, according to the theory described in section 3.2.3, should lead to larger particles. To keep the system stable and avoid total coagulation, an increased amount PVP were added as well.

On top of the more extreme conditions mentioned above, a batch of seeded polymerization, called PMMA-seeded, was synthesized as well. The principle being, that the second addition of reactants will prolong the growth stage, yielding larger and more monodisperse particles. The ingredients for the first and second stage are listed in Table 3.3

PMMA-seeded		
Ingredient	Weight, stage 1 (g)	Weight, stage 2 (g)
MMA	15	5
MAA/NaMA	0	1
PVP (65 kDa)	4	1
AIBN	0,4	0,025
MeOH	83	16

Table 3.3. List of ingredients used in the seeded polymerization of PMMA

The setup and temperature was the same as with the standard recipes, with the exception, that the second stage was added after 24 hours but the total reaction time remained 48 hours.

3.4 Analysis of the prepared PMMA particles

The analysis methods described below will apply to all particles throughout this work, unless otherwise stated.

3.4.1 Sizes

The particle sizes were measured on a Microtrac II – particle size analyser II and are reported here as the volume percentage of particles in different size classes, as well as the cumulative volume percentage. Further information on the equipment can be found in Appendix C. The median particle diameter is reported as d_{50}, the diameter at which the cumulative volume percentage reaches 50 %. The degree of polydispersity is reported as the geometric standard deviation (GSD), with a value of 1.1 being considered monodisperse, and is calculated from $GSD = (d_{84}/d_{16})^{½}$, as done in the work of Paine, 1990.

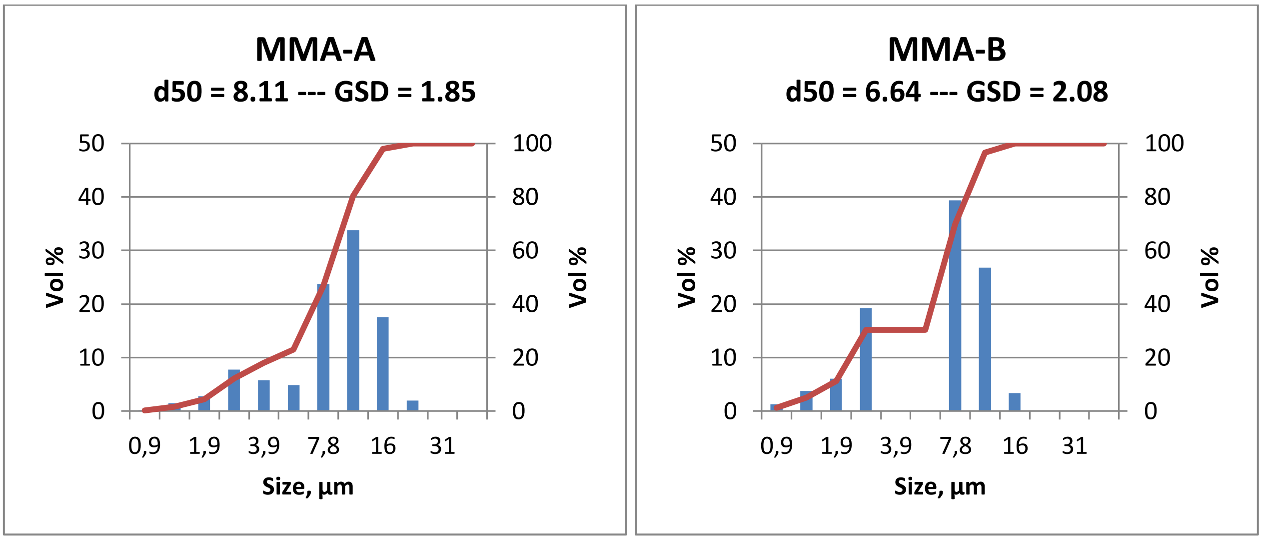

Fig. 3.9. Sizes obtained for PMMA-A and PMMA-B. Note that the cumulative percentage is displayed on a secondary axis.

Fig. 3.9 shows the measured sizes of the PMMA-A and PMMA-B particles as well as the d_{50} and GSD value. Monodispersity is not achieved and there are seemingly two different groups of particles sizes, one smaller fraction around 3 µm and one larger around 8-10 µm. The smaller particles of PMMA-B, compared to PMMA-A can be ascribed to the differences in the method used.

To confirm that the produced particles are spherical, SEM micrographs were taken of PMMA-A and PMMA-B. The micrograph of PMMA-A is seen in Fig. 3.10 and shows that the particles are indeed spherical as expected. Furthermore, it supports the measured size data from above with a group of smaller particles and a group of larger ones. It is assumed that particles from the other batches are spherical as well.

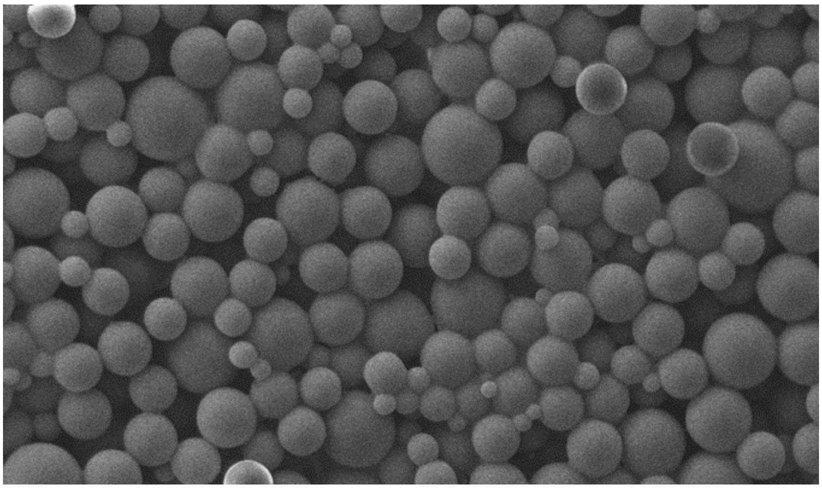

Fig. 3.10. SEM micrograph of the PMMA-A particles

The measured sizes from PMMA-C are displayed in Fig. 3.11 and is a broad distribution of different sizes ranging all the way from 1 µm to above 30 µm

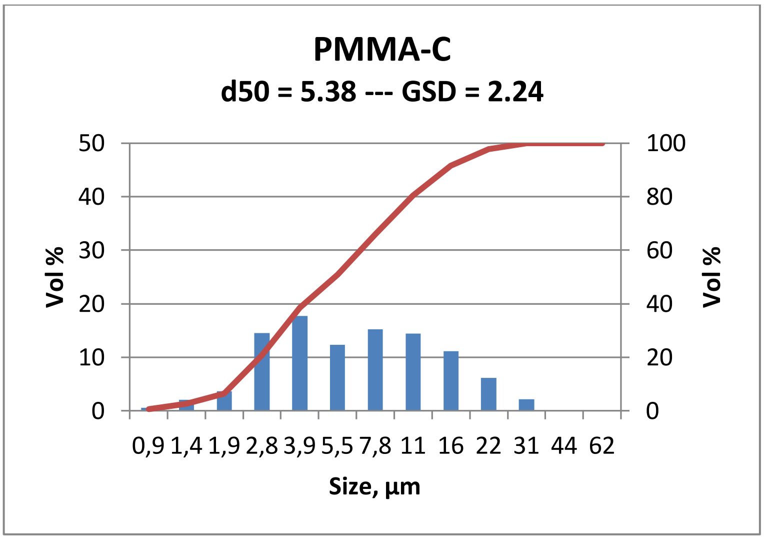

Fig. 3.11. Sizes obtained for PMMA-C. Note that the cumulative percentage is displayed on a secondary axis.

The sample taken from PMMA-seeded just before the addition of the second stage, were apparently not properly cleaned, as the particles sedimented in a non-reversible manner before any size measurements could be obtained. The final product was analyzed with the results shown in Fig. 3.12. The particles produced are significantly larger than the ones from the PMMA-B batch and the GSD is smaller, but there is still a group of smaller particles present, as seen in PMMA-A and PMMA-B.

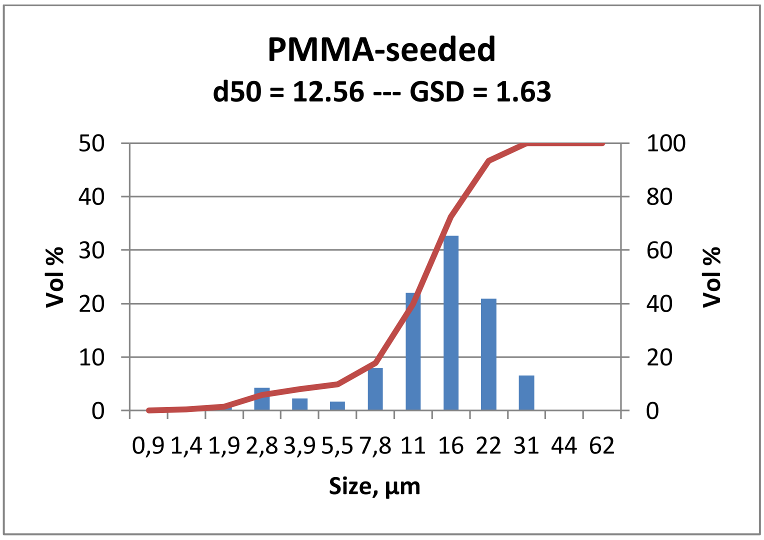

Fig. 3.12. Sizes obtained for PMMA-seeded. Note that the cumulative percentage is displayed on a secondary axis.

3.4.2 Charges

The amount of carboxylic acids on and inside the particle was measured by pH titration with 0.1 M NaOH. Further information about the equipment is available in Appendix C. A part of the original particle dispersion was diluted, with a 0.1 M aqueous $NaClO_4$ solution, to 20 mL with a dry matter content of approximately 6 g/L. The pH of the sample was then lowered to below 3, with a 0.1 M $HClO_4$ solution, prior to titration.

The resulting titration plots, an example of which, for PMMA-B, can be seen in Fig. 3.13 show no sign of any noticeable amount of carboxylic residue. Only the equivalence point of the strong acid $HClO_4$ is visible. This indicates that the co-polymerization with NaMA and MAA has been unsuccessful. This is also true for PMMA-A, PMMA-C and PMMA-seeded

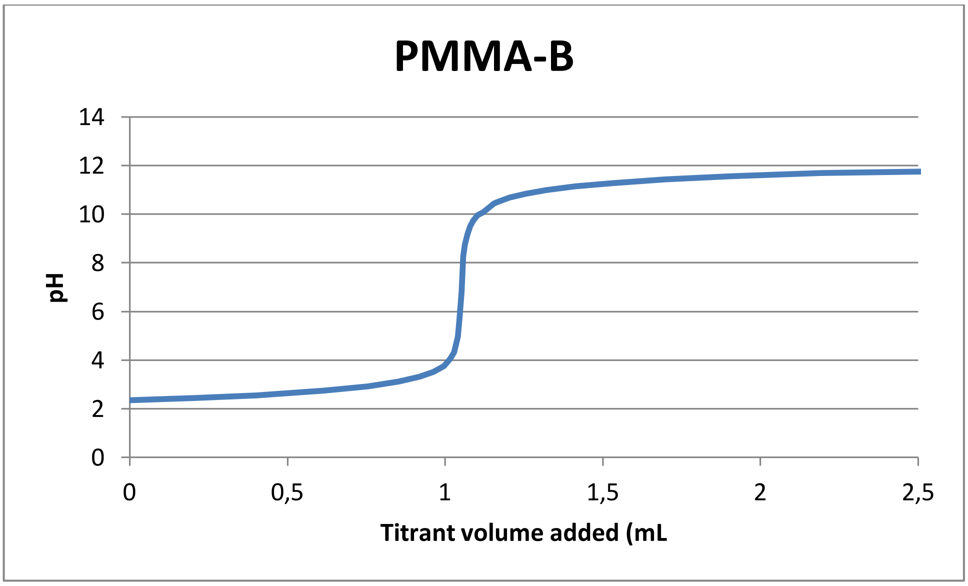

Fig. 3.13. pH titration of the PMMA-B particles

3.5 Challenges with the method in use

The produced particles, described in section 3.3 and 3.4 does not fulfill the aim of this work, as they are neither monodisperse nor charged, although the literature in general claim this to be possible(9). The following sections will present the challenges met, as well as give some ideas on how to solve them.

3.5.1 Keeping the particles monodisperse

As mentioned before, monodispersity is generally achieved by a higher growth rate of the smaller particles, relative to the larger ones. It can however be difficult to keep the system this way, since both secondary particle formation and large particle coalescence can occur, if the reaction parameters are not carefully controlled. To understand what happens, a more detailed view of, especially, the balance between the aggregation and stabilization processes is required.

Fig. 3.15 show a simulated overview of the dispersion polymerization process, with several properties of the particles and the system, plotted on a log-log scale, as a function of the degree of conversion. The numbers above the lines refer to the slope. These simulations and the graphs are part of the work done by Paine, 1990. In the simulations it is assumed, that stabilization is done entirely by the graft co-polymer, made from chain transfer to the stabilizer polymer, and that the produced graft is adsorbed immediately onto the particle surfaces. The production (and efficiency) of this graft co-polymer is not only directly affected by the factors mentioned in section 3.2.3, but also, to a large degree, the locus of polymerization, as it can only happen in solution. If the particles grow mainly by absorption of monomer, and hence solid phase polymerization within the particles, no grafted stabilizer can be produced. This locus of polymerization is, however, also more or less affected by these factors, making the control of the process even more complex. The graft co-polymer responsible for stabilization may, in the following sections, be referred to only as *graft.*

3.5.1.1 Simulation with a monodisperse product

The first graph, Fig. 3.14, is a simulation, where all the reaction parameters are correctly chosen/controlled, resulting in monodisperse particles. The point A is the point where the available graft exceeds the graft needed, Q_{min}, to avoid coalescence of similar sized particles or, in other words, where the particles become mature. After this point, the locus of polymerization is likely to shift from entirely solution polymerization, to a mix between solution and solid phase polymerization, with the latter being the dominant at a higher degree of conversion. This is indicated by a reduction of the slope of the line corresponding to the available graft. The particles will however remain monodisperse, as long as the available graft is within the band between Q_{min} and

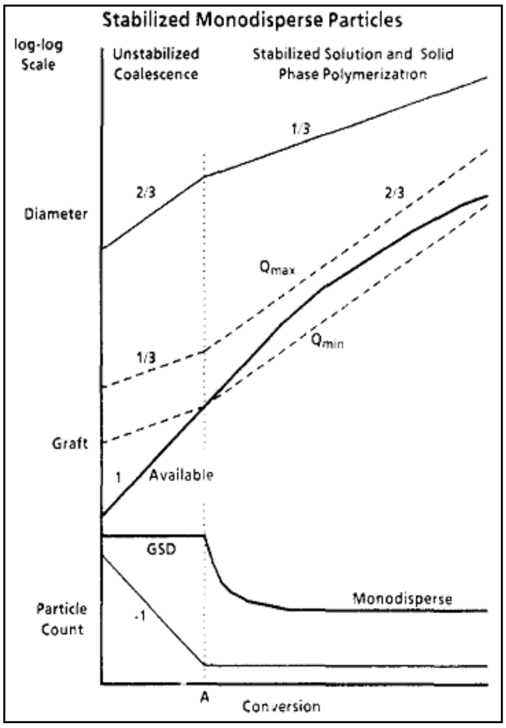

Fig. 3.14. Simulated overview of a dispersion polymerization process, resulting in monodisperse

Q_{max}, with the latter being the maximum amount of grafted stabilizer it is possible to fit on the particle surface. A further explanation of these terms is given in section 3.5.1.4. (10)

Choosing reaction conditions, not within the boundaries of those giving the situation outlined above, would result in a polydisperse final product or, in the extreme case, total coagulation. This complies well with the observation made, when trying to produce particles under more extreme conditions than normally found in literature, as in section 3.3. In the case of a polydisperse final product, two things can happen as illustrated in Fig. 3.15.

3.5.1.2 Simulation with secondary particle formation

The left part (Fig. 3.15 A) is a simulation of a dispersion polymerization process where solution polymerization remains dominant throughout the entire reaction time. The slope of the available graft will remain 1 and eventually reach Q_{max} at point B_1. The already mature particles can then no longer adsorb the produced graft, and the graft will instead adsorb to the smaller nuclei being produced as a product of solution polymerization. Under normal conditions, the larger particles can only scavenge the nuclei because they are not yet stabilized, so when this happens, the scavenging stops, and a new population of small mature particles will appear. This is shown by a jump in particle count along with a corresponding jump in Q_{min} and Q_{max}, as the total surface area will increase as well. This can happen several times (point B_2) during the reaction, giving rise to several populations of particles each with their own class of sizes.(10)

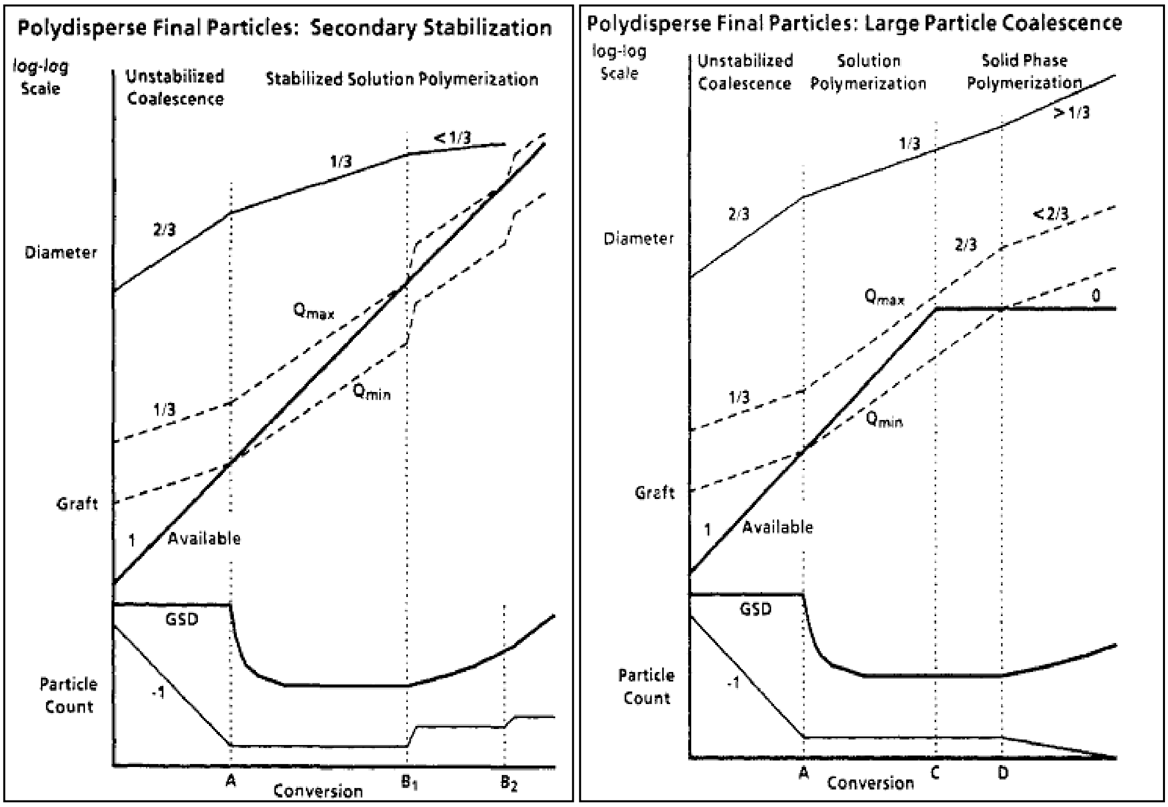

Fig. 3.15. Simulated overview of a dispersion polymerization process, resulting in polydisperse particles due to: A- secondary stabilization (left) and B- large particle coalescence (right) (9)

3.5.1.3 Simulation with large particle coalescence

The right part (Fig. 3.15 B) is the opposite situation where the solid phase polymerization becomes to dominant too soon (point C), greatly limiting the production of grafted stabilizer, as indicated with a slope of 0 in the extreme case, with no graft being produced at all. The particles will continue to grow, by absorption of monomer and subsequent solid phase polymerization, until the surface area of the particles becomes too large and Q_{min} exceeds the graft available at point D. The particles will then become unstable again, as in the beginning of the process, and coalescence will occur, reducing particle count.(10)

3.5.1.4 Estimating Q_{min} and Q_{max}

If the above mentioned simulations should be of any proper practical value, an estimate of Q_{min} and Q_{max}, for the system in use, will be needed. According to Paine, 1990, the value of Q_{min} is thought to be linked to the area projected on the particle surface by the hemisphere defined by the radius of gyration, r_g, of the stabilizer polymer in solution. So when the sum of projected areas equals the surface area of the particle, the particle is assumed to be stable.

The radius of gyration can be calculated as $r_g = a \cdot M_w{}^b$, with a being a proportionality constant, M_w being the molecular weight of the stabilizer polymer and b being the exponent relating M_w to r_g. a and b are material dependent and can be measured experimentally The values used here are taken from literature as $a = 5.3 \cdot 10^{-8}$ and $b = 0.32$, both in MeOH(18). Significantly lower values of rg have been reported (19), but are not considered here. Since the chain transfer can happen anywhere on the stabilizer chain, r_g of the grafted stabilizer will, on average, be 75 % of that of the ungrafted stabilizer, leading to $r_g = a(0.75M_w)^b$. Q_{min} is then given by $1/\pi r_g{}^2$ with the units of grafts pr m^2. (10) The PVP used in section 3.3 has a molar weight of 60 kDa giving a r_g of 16.3 nm and a Q_{min} of approximately 1200 grafts/µm^2 as opposed to 14.6 nm and 1500 grafts/µm^2 for the 40 kDa PVP used in the referred work of Paine, 1990.

Since the main problem, under the normal conditions used in section 3.3, is secondary particle formation, especially Q_{max} will be of interest. It is estimated to be approximately 10 times larger than Q_{min}, as the good solubility of PVP in methanol allows the PVP chains to extend further from the surface, allowing a higher density of grafts on the particle surface.(10) This is shown graphically in Fig. 3.16, where, at Q_{min}, the individual PVP chains will be held close to the particle surface, whereas, at Q_{max}, the chains will extend much further form the particle surface.

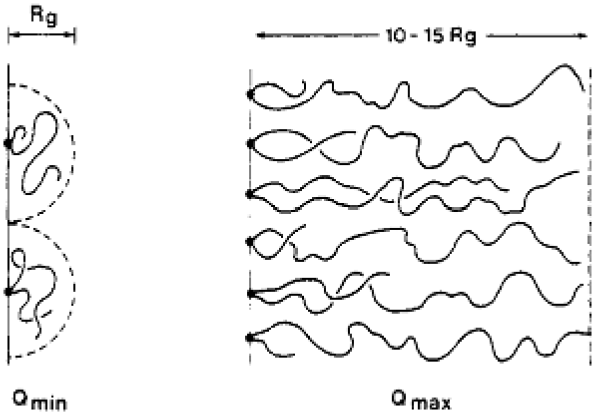

Fig. 3.16. Schematic representation of the relative orientation of stabilizer chains grafted onto the particle surface by chain transfer. The drawing is not to scale.(10)

By using the Q_{min} of the 60 kDa PVP, it can be calculated, that the minimum amount of grafted PVP needed per m^2, to avoid coalescence of similar sized particles, is 0.12mg/m^2. For a batch of particles produced from 20 mL styrene with a particle diameter of 5 µm, the total surface area will be close to 21 m^2. The minimum amount of grafted PVP for such a batch will then be 2.5 mg. If the probability of chain transfer is approximately 1 in every 100 PVP chains, as estimated by (10), the amount of PVP (60 kDa) used in a batch from 20 mL styrene should be between 0.25 and 2.5 g to keep the particles monodisperse.

3.5.1.5 Testing the estimation

Unfortunately it was not possible to find an estimation of the probability of chain transfer when using MMA, but the maximum amount of grafted PVP is calculated to be 17 mg for a batch made from the recipes of PMMA-A and PMMA-B in section 3.3, or 23 mg if using 20 mL monomer instead. If the chain transfer probability is in the same range as with PVP/styrene this would indicate that too much PVP were used in these recipes. This is consistent with the observation of secondary particle formation. A series of experiments were conducted to investigate the effect of a lower amount of PVP, all ending in massive coagulation within the first 30 minutes after the initial particle formation stage. It seems that the process of dispersion polymerization using MMA is less well behaved than when using styrene. Firstly, the chain transfer probability can probably be assumed to be less than 1:100, as all attempts to use less PVP than in the recipes of PMMA-A and PMMA-B failed very early in the process, indicating that the graft available never reached Q_{min}. Secondly, solution polymerization might be more favored in the later part of the process when using MMA compared to similar recipes using styrene.

Even though the point A, in Fig. 3.14 and Fig. 3.15, is not as sharp in reality as it is defined here, the window of particle formation is still very short compared to that of particle growth. The increase in total surface area as a function of conversion, dA_p/dx, will therefore be very high in the beginning of the process, before 1 % conversion is obtained. Since Q_{min}, and Q_{max} is proportional to the total surface area, a lot of graft will have to be produced within this window of time to keep the system from total coagulation. Even though the simulations only take the grafted stabilization into account, which might not be at correct assumption, there is still a tendency to an overproduction of graft at the end, if the PVP concentration is as high as needed in the beginning. This could be overcome by adding a co-stabilizer which will adsorb more strongly than ungrafted PVP, thus enabling a lower concentration of PVP. Another solution could be to use a macromonomer with stabilizing properties, making a comb/brush polymer by the co-polymerization with the normal monomer, allowing the comb/brush polymer to adsorb very strongly to the particle, or even anchor to the particle if the branches are far enough from each other (20). An example of a comb/brush polymer is shown in Fig. 3.17, with every fourth unit in the backbone being a macromonomer.

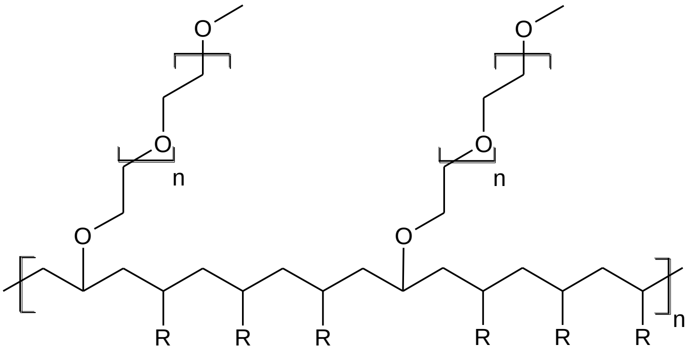

Fig. 3.17. Schematic representation of a comb/brush polymer

3.5.2 Implementing charges on the surface

Particle charge is probably one of the most important properties needed for the purpose of this work. The lack of co-polymerization with MMA/MAA/NaMA was unexpected and unfortunate, as this could have resulted in particles, where the charge and water swellability, could have been adjusted by changing the pH value.

3.5.2.1 Using a higher fraction of MAA

Three syntheses, using the same recipes and method as in section 3.3, with a few exceptions stated below, but with an increased amount of MAA relative to MMA, were conducted to see if this would yield particles with the properties in question. An overview of the batches can be found in Table 3.4.

MMA:MAA (mol)	Weight of MAA (g)	Charges	Size / GSD	Coagulation
1:0.03	0.387	None	11.3 µm / 2.07	Small
1:0.05	0.645	None	20.3 µm / 1.44	Medium-high
1:0.07	0.903	None	-	Total

Table 3.4. An overview of three batches made to determine the influence of an increased MAA content

Prior to this, the AIBN had been recrystallized in methanol to remove some insoluble residue. Furthermore, the MMA were used without removal of the inhibitor, as this will slow the onset of particle formation, ensuring that the temperature is allowed to rise again after the addition of the AIBN solution. This will have affected the results in such a way, that the batch with the same molar ratio of as that in PMMA-B, have produced significantly larger particles than before, which, however, also could be caused by the fact that the PMMA-B batch were heated after addition of AIBN, whereas this batch were heated before.

Apart from that, no acidic groups were found by titration, and an increase in the MAA fraction seems to have the same effect as reducing the PVP content, when regarding size and amount of coagulation. The GSD decreased when going from 1:0.03 to 1:0.05, which is due to a much smaller degree of secondary particle formation with the higher fraction of MAA, again showing the same effect as when reducing the PVP content.

These findings stand in contrast with the work done by Kun, et al., 2000, where too much MAA increased secondary stabilization and where the acidic groups were both adsorbed and anchored to the particle surface, as well as buried within the particle core. The only difference is that Kun, et al., 2000 used a mixture of methanol and water in a 7:3 weight ratio, which, however, might explain the additional stabilizing effect, as this will make the system resemble emulsifier free emulsion polymerization a bit more. This will shift the locus of the polymerization of MMA more towards the solid phase (especially in the later stages), whereas the MAA will continue to have a higher solubility in the continuous phase, generating chains with a much higher fraction of MAA subunits.

The batches made in this work does not contain any water, and it is suspected, that the reaction shown in Fig. 3.18, between PVP and MAA, can occur, with the former being a weak base and the latter being a weak acid.

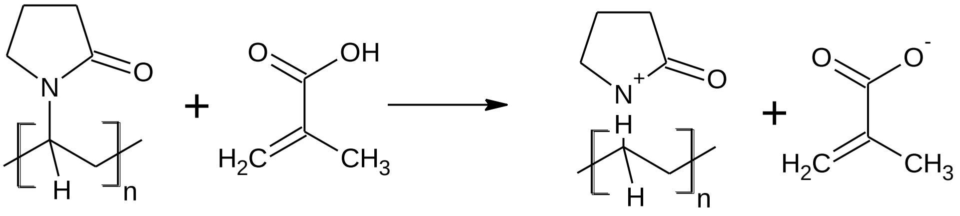

Fig. 3.18. Suspected reaction between PVP and MAA

If the MAA is able to protonate some of the subunits in the PVP polymer, creating a salt where the MAA is associated to the PVP subunit, then the diffusivity of MAA will be greatly reduced and with it, the chance of incorporation. The protonated PVP subunit will, furthermore, render the α-hydrogen inactive, reducing the chance of chain transfer. At the end of the reaction, the cleaning process will remove most, if not all, of the added MAA.

It is unknown why the NaMA in PMMA-A is not incorporated into the particles, but since it is a salt, it might not be soluble enough in the polymer, making up the particles, to be efficiently incorporated, and could therefore be removed during the cleaning process.

3.5.2.2 Polyacrylic acid as stabilizer

In section 3.2.2, PAA is mentioned as a possible stabilizer, with the same general grafting mechanism as PVP. PAA does also contain an active α-hydrogen and is as such prone to chain transfer as well. The use of PAA instead of PVP has the advantage that the particles will have a charged shell, even without the use of MAA as a co-monomer. The particle core will however not be affected and the particles will have a higher resemblance of those made by Hinge, et al., 2006

All attempts of using PAA as stabilizer in combination with MMA failed, regardless of the PAA concentration. It was then found that styrene has a higher chain transfer rate, to some compounds, than MMA (16), which was also indicated by the results discussed in section 3.5.1.5, making the PS/PAA couple a possible candidate instead.

The drawback, of this method to introduce charges, is that the charge density can be hard to control and is probably linked with particle size, making particles with varying size/charge density ratios hard to obtain in a controlled manner.

3.6 Preparation of PAA stabilized PS particles

A new set of synthesis were conducted, with the general aim being the same as in section3.3, except for the co-polymerization with MAA. This time, styrene was the main monomer and PAA the stabilizer.

All the ingredients, except AIBN, were mixed in a 250 mL two-necked round-bottomed flask equipped with a magnetic stirrer and heated to reaction temperature while being purged with nitrogen. At the same time, the AIBN was dissolved in 10 mL methanol at room temperature, and purged with nitrogen for the same time as the main mixture. When the reaction temperature was reached, the AIBN solution was added to the main mixture and kept under nitrogen atmosphere. After approximately 24 hours, when the mixtures no longer smelled of styrene, the conversion was assumed complete and any remaining free radicals were quenched by addition of 5 mL 50 g/L hydroquinone solution in methanol. The cooled dispersions were cleaned, as in the other synthesis, by a repeating sedimentation/redispersion process in methanol. All the chemicals were used as received, except AIBN, which were recrystallized in methanol before use.

At first a PAA with a molecular weight of 25 kDa were used with mixed results. Generally, a lot of coagulation occurred, but at higher stabilizer concentrations it was possible to salvage some of the particle dispersion. Two of the batches yielded a recoverable amount. These are called, PS-A and PS-B and the reaction conditions can be found in Table 3.5 and Table 3.6

PS-A (60 °C)	
Ingredient	Weight (g)
PS	15
PAA (25 kDa)	4
AIBN	0.2
MeOH	80.4

Table 3.5. Reaction conditions for PS-A

PS-B (70 °C)	
Ingredient	Weight (g)
PS	18
PAA (25 kDa)	6
AIBN	0.2
EtOH	79

Table 3.6. Reaction conditions for PS-B

Then a PAA with a molecular weight of 100 kDa, as a 35 w/w % solution in water, were used for the batches called PS-C and PS-D, with the reaction conditions found in Table 3.7 and Table 3.8. For these batches, no coagulation at all was observed.

PS-C (60 °C)	
Ingredient	Weight (g)
PS	20
PAA (100 kDa)	3.5
AIBN	0.3
MeOH	100
Water (from PAA)	6.5

Table 3.7. Reaction conditions for PS-C

PS-D (60 °C)	
Ingredient	Weight (g)
PS	25
PAA (25 kDa)	3.5
AIBN	0.3
MeOH	100
Water (from PAA)	6.5

Table 3.8. Reaction conditions for PS-D

3.7 Preparation of PAA and macromonomer stabilized PS

In section 3.5.1.5, it was stated that the use of a macromonomer with stabilizing properties, could help keeping the system stable during the initial phases of the dispersion polymerization process. In order to test if this statement is true, such a macromonomer would first have to be synthesized, as the commercially available products are very expensive, in addition to being of relatively low molecular weight.

It was decided to combine a monomethyl ether PEG (5 kDa) with methacrylic anhydride, creating a PEGMA macromonomer. This is done by esterification of the hydroxyl group on the PEG, with Pyridine as base and dimethylaminopyridine (DMAP) as nucleophilic catalyst. The chemicals used for this can be found in Table 3.9.

PEGMA	
Ingredient	Amount
PEG (5 kDa)	25 g
Methacrylic anhydride	4 mL
Pyridine	20 mL
DMAP	6.1 g
Dichloromethane	150 mL

Table 3.9. List of chemicals used in the synthesis of PEGMA

All of the ingredients were mixed in a 250 mL two-necked round-bottomed flask, equipped with a magnetic stirrer, purged with nitrogen for 20 min, and heated to 60 °C. The mixture was then allowed to stand at this temperature, in nitrogen atmosphere, for 72 hours. The product and any unreacted PEG's, was precipitated with diethyl ether at room temperature, redissolved in chloroform and precipitated again to minimize pollution by pyridine and DMAP.

The synthesized PEGMA were used along with PAA (25 kDa), with the reaction conditions shown in Table 3.10. No coagulation was observed.

PS-co-P(PEGMA) (60 °C)	
Ingredient	Weight (g)
PS	20
PAA (25 kDa)	4
PEGMA	4
AIBN	0.3
MeOH	100

Table 3.10. reaction conditions for PS-co-P(PEGMA)

3.8 Analysis of the prepared PS particles

All of the PS particles were analyzed with regard to size and charge by the same methods as described in section 3.4.

3.8.1 Size

Fig. 3.19 to Fig. 3.22 show the particle sizes and GSD for the individual batches of PS particles.

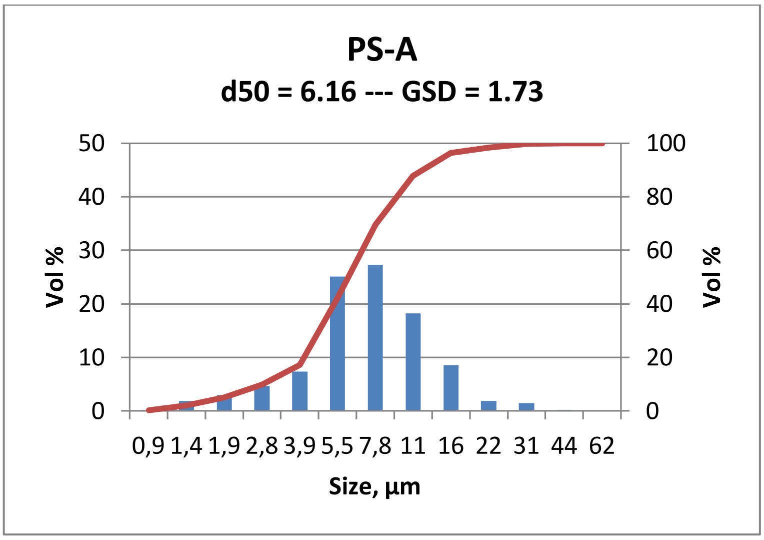

Fig. 3.19. Sizes obtained for PS-A. Note that the cumulative percentage is displayed on a secondary axis.

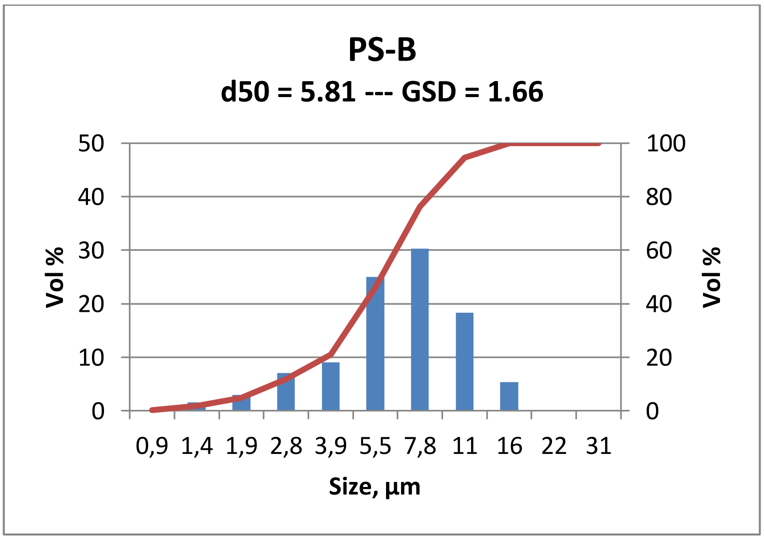

Fig. 3.20. Sizes obtained for PS-B. Note that the cumulative percentage is displayed on a secondary axis.

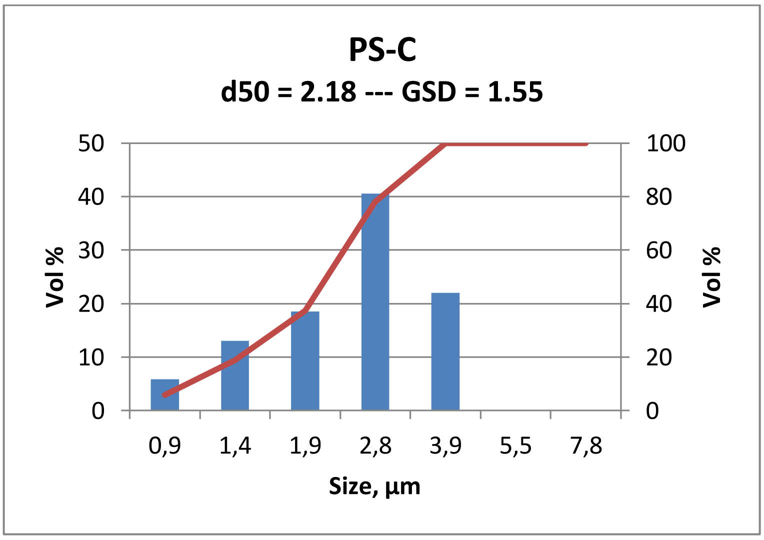

Fig. 3.21. Sizes obtained for PS-C. Note that the cumulative percentage is displayed on a secondary axis.

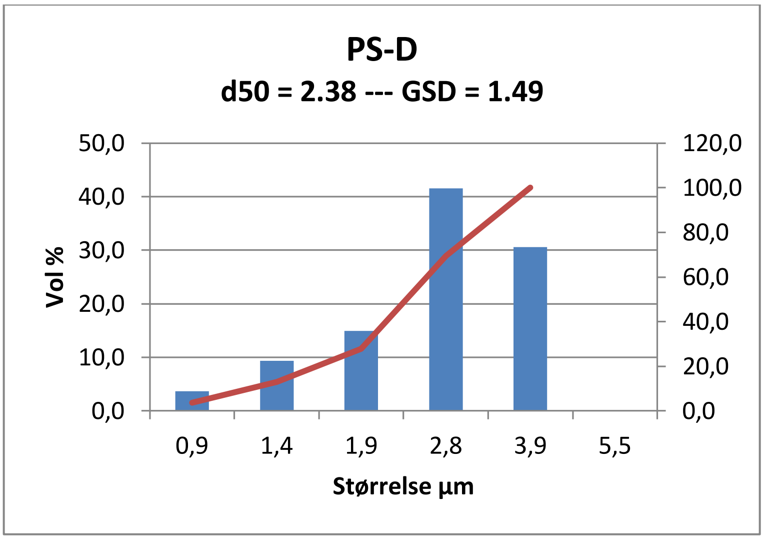

Fig. 3.22. Sizes obtained for PS-D. Note that the cumulative percentage is displayed on a secondary axis.

Reservation must be taken when comparing the particle size obtained in PS-A and PS-B with PS-C and PS-D, as the two former still contained a lot of coagulated material making the recipes unreliable and inefficient.

As for the particles from the PS-co-P(PEGMA) batch, the size analysis are shown in Fig. 3.23. The effect of the PEGMA is clear, as both particle size and GSD are a lot smaller than those from the, otherwise partly comparable, batch of PS-A.

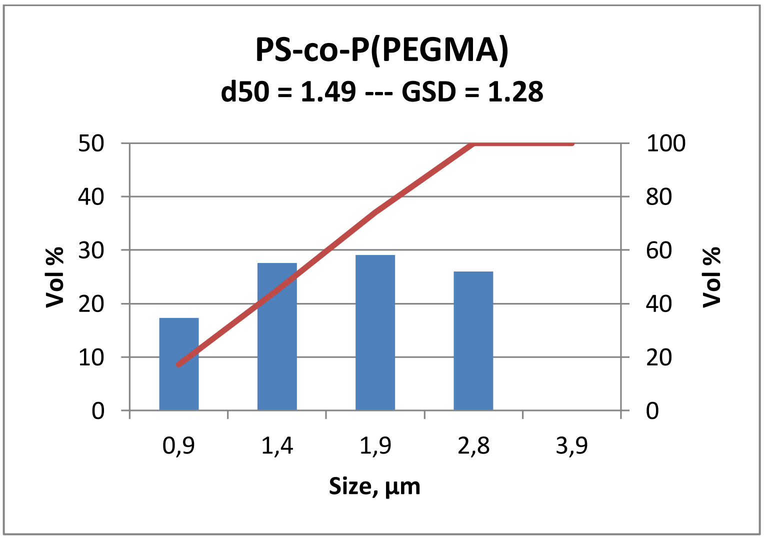

Fig. 3.23. Sizes obtained for PS-co-P(PEGMA). Note that the cumulative percentage is displayed on a secondary axis.

3.8.2 Charges

All of the PS particles have negatively charged groups from the grafted PAA stabilizer. An example of a pH titration plot is shown in Fig. 3.24, for the titration of PS-D with the same method as described in section3.4.

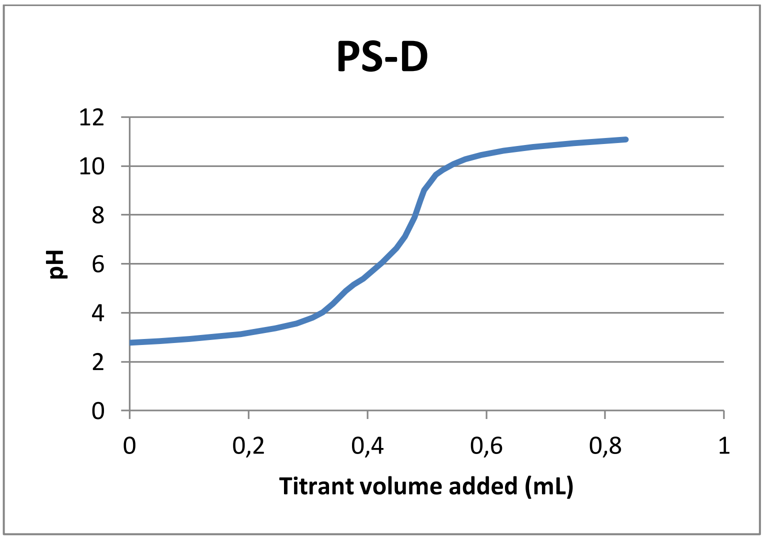

Fig. 3.24. pH titration of PS-D

Since the equivalence points are difficult to see directly, the second derivative, d^2pH/dV^2, can be plotted as a function of the volume added, as shown in Fig. 3.25. Here the equivalence points can be calculated from the intersection with the x-axis, but only when going from positive to negative values. The charge density, in eq/m^2, can then be calculated by using Eq. 3-1, where V_{eq1} and V_{eq2} is the titrant volume used at the first and second equivalence point respectively, $C_{titrant}$ is the molarity of the titrant, V_{sample} is the volume of the sample prior to titration, s is the dry matter content of the sample in g/L and A_{spec} is the weight specific area of the particles in the sample in m^2/g dry matter.

$$charge\ density = \frac{\left(V_{eq2} - V_{eq1}\right) * C_{titrant}}{V_{sample} * s * A_{spec}}$$

Eq. 3-1

Plots resembling these were obtained for all the titrated PS particles (PS-C, PS-D and PS-co-P(PEGMA)) and their charge density summarized in Table 3.11 PS-A and PS-B was not titrated, due to the low amount of obtained material.

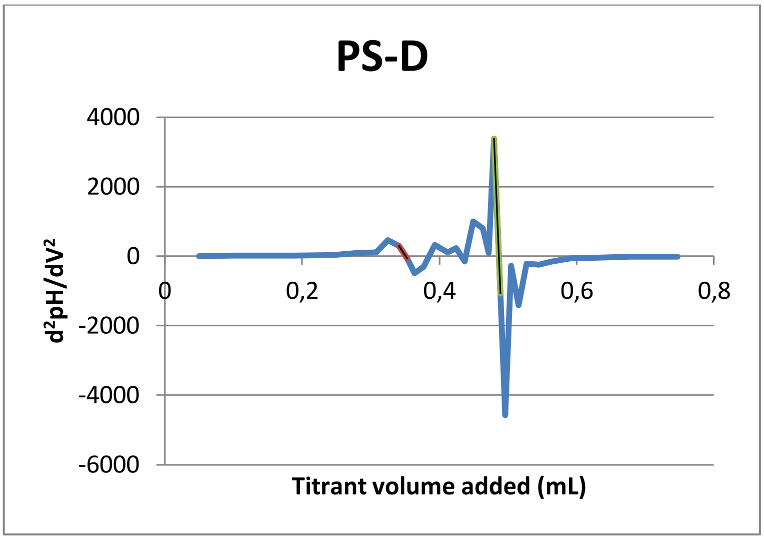

Fig. 3.25. The second derivative (d^2pH/dV^2) plotted against titrant volume for the pH titration of PS-D

Name	Charge density (mEq/m^2)
PS-C	0.010
PS-D	0.020
PS-co-P(PEGMA)	0.042

Table 3.11. The charge densities calculated from pH titration of PS particles.

3.9 Summarization of the results from dispersion polymerization

A lot of interesting and somewhat surprising results were obtained from the dispersion polymerizations carried out during this project. A summary of the properties and some of the reaction conditions is found in Table 3.12 and Table 3.13.

Name	Solvent	Stabilizator	Conc, stabilizator *	Conc, monomer **
PMMA-A	MeOH	PVP(60 kDa)	26,7	13,6
PMMA-B	MeOH	PVP(60 kDa)	26,7	13,6
PMMA-C	MeOH	PVP(60 kDa)	30	18,8
PMMA-seeded	MeOH	PVP(60 kDa)	25,3 (total)	14,4 (total)
PS-A	MeOH	PAA(25 kDa)	26,67	14,6
PS-B	EtOH	PAA(25 kDa)	33,33	16,7
PS-C	EtOH	PAA(100 kDa)	17,5	15,8
PS-D	EtOH	PAA(100 kDa)	14	19
PS-co-PEGMA	EtOH	PAA(25 kDa) + PEGMA	20 + 20	16,7

Table 3.12. Selected properties and reaction conditions of the particles produced.
* Wt. % of monomer, ** Vol. % of total liquids, *** d50

Name	Conc, co-monomer *	Conc, AIBN *	Size, µm ***	GSD	Charge (mEq/m^2)
PMMA-A	2,5 (NaMA)	1,33	8,11	1,85	0
PMMA-B	2,5 (MAA)	1,33	6,64	2,08	0
PMMA-C	2,5 (NaMA)	3	5,38	2,24	0
PMMA-seeded	5 (NaMA)	2 (total)	12,56	1,63	0
PS-A	0	1,33	6,16	1,73	Not measured
PS-B	0	1,1	5,81	1,67	Not measured
PS-C	0	1,5	2,18	1,55	0.010
PS-D	0	1,2	2,38	1,49	0.020
PS-co-P(PEGMA)	0	1,5	1,49	1,29	0.042

Table 3.13. Selected properties and reaction conditions of the particles produced.
* Wt. % of monomer, ** Vol. % of total liquids, *** d50

The particles produced from PMMA/PVP were all larger than the PS/PAA particles, although they were also less monodisperse due to secondary particle formation. Due to lack of time, larger particles were not obtained by the PS/PAA way, but it should be theoretically possible. It is not known whether recipes with PS/PAA yielding larger particles, will show the same tendency of secondary particle formation as with PMMA/PVP.

When using PMMA/PVP there seems to be some maximum obtainable particle sizes, as almost all attempts with more extreme conditions ended in total coagulation relatively fast. In the only case where stable particles were obtained, PMMA-C, the size were smaller and the size distribution wider than for both PS-A and PS-B. The Issue seems to be that, in order to achieve sufficient stabilization in the beginning of the process, the PVP concentration has to be so high, that separate groups of particles with different sizes will appear, due to secondary stabilization.

It was speculated that the addition of a co-stabilizer or a macromonomer with stabilizing properties, could reduce this problem. By comparing PS-A with PS-co-P(PEGMA), this seems indeed to be the case. PS-A produced larger particles along with an unacceptable amount of coagulum, while PS-co-P(PEGMA) produces smaller particles with a narrower size distribution and no coagulum at all. This promises well for the speculation, but more experiments will have to be conducted to find some consistency in this.

In addition to this, the PS-co-P(PEGMA) particle is believed to have a different morphology in comparison with the other PS particles. This is because the co-polymerization of styrene and PEGMA is likely to produce a much denser “hairy” layer of PEG-chains around the particle, while still keeping the longer chain transfer grafted PAA-chains. If this assumption is true, the particle might look like the one sketched in Fig. 3.26, with the black lines being PAA and the red ones being PEG.

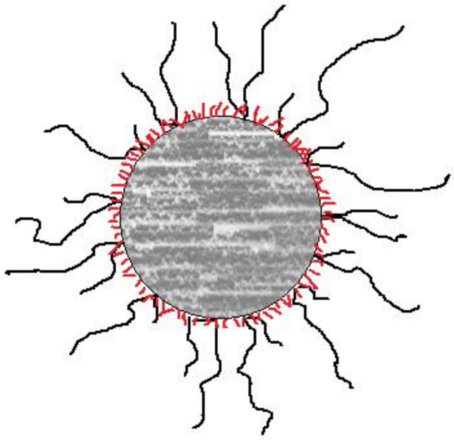

Fig. 3.26. Drawing of a possible morphology of the PS-co-P(PEGMA) particles. Note that the proportions are not to scale.

The attempts to co-polymerize MMA with MAA and NaMA, respectively did all fail, as no titratable acidic groups were found on or in the particles. It is thought that the MAA might react with PVP, making the PVP less active for chain transfer and creating an association between the PVP polymer and the MAA, keeping the MMA form being incorporated into the particle. It is, however, not known why NaMA does not co-polymerizes, as it should not react with PVP in the same way as MAA, although it is speculated that the solubility of the sodium salt in the main polymer is too low for it to be incorporated efficiently.

All of the PS particles were charged due to the grafted PAA stabilizer, but the charge density varies amongst the different batches. Even between PS-C and PS-D there is a factor two difference, even though the only difference in the recipes is a larger fraction of monomer in PS-D. According to the mechanism of stabilization, the increased monomer concentration should actually have the opposite effect, tending to produce larger, but less stabilized particles. If this is simply a coincidence, or if there is something in the particle growth mechanisms that still are less understood is not clear, and a more controlled set of experiments will be required to investigate this further. The difference could also simply be caused by inaccuracy in the pH-titrations, as the titrations were performed under normal atmosphere, since bubbling with nitrogen left the sample foaming and spilling over the beaker. In addition, the PAA stabilized particles tends to become unstable at low pH and some coagulation were observed. The coagulated masses was however redispersed during the titrations, when pH were increased above 4, so the coagulation was, at first, not assumed to be of great effect. This assumption might, however, be false, as the charge density of PS-co-P(PEGMA) is even higher, although the smaller particles will have a larger specific surface area. If the chain transfer rate is approximately the same for all batches the larger specific surface area should decrease the charge density. Since the dense inner layer of PEG-chains on the PS-co-P(PEGMA) particles will have some stabilizing effect, regardless pH, the sample will be less likely to coagulate at low pH. The higher charge density of PS-co-P(PEGMA), compared to the other PS particles, can thus indicate, that the coagulation observed is not totally reversible, trapping some of the acidic groups inside the coagulated mass.

All in all, dispersion polymerization might still be a promising candidate for producing particles with the wanted properties, but a higher understanding of the different processes during the particle formation and growth stages are required, as they appear to be very complex. This can be obtained by a larger set of experiments with more controlled settings, so that the parameters of the wanted properties can be investigated one by one.

4 Part two – Filtration dewatering of the synthesized particles

This part will focus on how the synthesized model particles, from section 3, behave during a filtration dewatering process and will involve some general theory and mathematical models of filtration processes.

4.1 Filtration theory

The starting point when regarding a filtration process is the flux equation, Eq. 4-1. Here J_i is the flux inside the pores, μ is the liquid viscosity, R is the specific resistance and dP_l/dl is the liquid pressure gradient.(4)

$$J_i = \frac{1}{\mu \cdot R} \frac{\mathrm{dP_l}}{\mathrm{dl}}$$

Eq. 4-1

In the simplest of situations, the resistance will be composed only of the membrane resistance, but as soon as material begin to deposit on top of the membrane, the additional resistance of the filter cake will have to be taken into account. Under most circumstances, the membrane resistance will be small and constant (except when the pores become partially or totally blocked by adsorption inside the pore) and can be neglected.(3)

As the liquid flow through the filter cake, the drag generated causes the liquid part of the pressure to reduce, while the solid pressure, P_s, exerted by the particles, is increased in such a way that: $P_e = P_l + P_s$, with P_e being the external pressure applied. Under ideal conditions, when the filter cake consists of monodisperse, spherical and non-compressible particles, the cake will be uniform in every way from top to bottom. This causes the pressure gradient to be the same everywhere along the length/height of the cake, leading to the following relationship: $-dP_l/dl = P_e/L$, with L being the total length/height of the cake. This relationship is also illustrated in Fig. 4.1.(4)

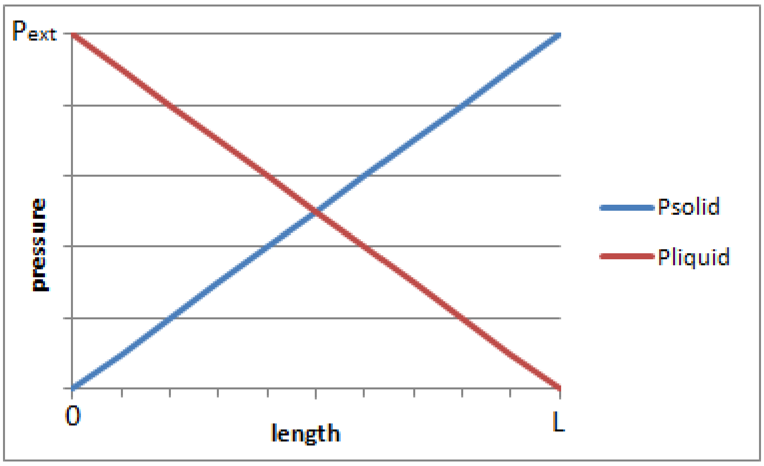

Fig. 4.1. The relationship between Ps and Pl

The flux inside the pores is also a description of the liquid velocity, assuming that the flow is laminar. This value is normally of no practical use, but can be converted to the "empty tower velocity", equal to the flux over the entire membrane surface, J. This is done by multiplying J_i

with the porosity of the filter cake, defined by, $\varepsilon = V_{void}/V_{total}$. Applying this to Eq. 4-1 and introducing $R' = R/\varepsilon$, will give Eq. 4-2

$$J = \frac{1}{\mu \cdot R'} \cdot \frac{P_e}{L}$$

Eq. 4-2

The resistance term will depend on the cross sectional area of the pores, through which the liquid will flow down through the cake. These pores can be treated as small, parallel and circular tubes, where the Hagen–Poiseuilles equation will apply (21). In a cylindrical tube, the cross sectional area is proportional to the square of the cylinder radius, which can be calculated as the ratio between the cylinder volume and the surface area of the cylinder wall. For the pores in the cake, the average pore radius, r_p, can thus be assumed to be proportional to the ratio between the pore volume and the pore surface area. Assuming that the pore surface area is identical to the total surface area of the particles in the filter cake and utilizing that the volume specific particle area, $S_0 = A_p/V_p$, the average pore radius can be calculated by Eq. 4-3 with A being the area of the membrane.

$$r_p = k \cdot \frac{A \cdot L \cdot \varepsilon}{S_0 \cdot A \cdot L \cdot (1-\varepsilon)} = k \cdot \frac{\varepsilon}{S_0 \cdot (1-\varepsilon)}$$

Eq. 4-3

Inserting the expected dependency of the cross sectional pore area on the resistance will then give Eq. 4-4, which is the Kozeny-Carman equation (3) and can be used to predict the resistance as a function of particle size. By combining Eq. 4-2 with Eq. 4-4, to Eq. 4-5, the Kozeny-Carman equation can then be used to predict the flux. The Kozeny-Carman coefficient, k_c, is typically taken to be 5 for uniform spheres (3).

$$R' = \frac{R}{\varepsilon} = k' \frac{1}{{r_p}^2 \cdot \varepsilon} = k_c \cdot \frac{{S_0}^2 \cdot (1-\varepsilon)^2}{\varepsilon^3}$$

Eq. 4-4

$$J = k_c \cdot \frac{\varepsilon^3}{\mu \cdot {S_0}^2 \cdot (1-\varepsilon)^2} \cdot \frac{P_e}{L}$$

Eq. 4-5

4.1.1 Dead end filtration

In dead end filtration, the cake height, L, will increase with time, t, but since L is difficult to obtain experimentally, the material coordinate, $\omega = s \cdot V_f/A$, is typically used instead as $d\omega = \rho_p \cdot (1-\varepsilon) \cdot dl$, transforming Eq. 4-2 to Eq. 4-6. (4)

$$J = \frac{\varepsilon \cdot \rho_p \cdot (1-\varepsilon)}{\mu \cdot R} \cdot \frac{P_e}{\omega}$$

Eq. 4-6

A new resistance term, α, is now introduced as $\alpha = R/(\varepsilon \cdot \rho_p \cdot (1 - \varepsilon))$ giving Eq. 4-7

$$J = \frac{1}{\mu \cdot \alpha} \cdot \frac{P_e}{\omega}$$

Eq. 4-7

Inserting the same dependency of r_p on R as before, will give Eq. 4-8, a variant of the Kozeny-Carman equation, using material coordinates. It is important to notice, that the units of R' and α are not the same.

$$\alpha = k_c \cdot \frac{{S_0}^2 \cdot (1 - \varepsilon)}{\rho_p \cdot \varepsilon^3}$$

Eq. 4-8

The flux also can be describes in terms of volume as in Eq. 4-9, which, in combination with Eq. 4-7, remembering that $\omega = s \cdot V_f / A$, will give Eq. 4-10

$$J = \frac{1}{\varepsilon \cdot A} \cdot \frac{dV_f}{dt}$$

Eq. 4-9

$$\frac{dV_f}{dt} = \frac{A^2 \cdot P_e}{\alpha \cdot s \cdot V_f}$$

Eq. 4-10

This will, upon rearrangement and integration, give Eq. 4-11 which can be used to calculate the specific resistance from experimental data, as a plot of t/V_f *vs.* V_f should give a straight line with a slope of $\mu \cdot \alpha \cdot s / P_e \cdot 2A^2$. Such a plot is commonly called a Ruth-plot.(4)

$$t = \alpha \cdot \frac{\mu \cdot s \cdot {V_f}^2}{P_e \cdot 2A^2} <=> \frac{t}{V_f} = \alpha \cdot \frac{\mu \cdot s \cdot V_f}{P_e \cdot 2A^2}$$

Eq. 4-11

The measured specific resistance can then be compared to the one obtained from the Kozeny-Carman relation.

The effect of the osmotic pressure in the filter cake has deliberately been omitted, as this normally only play a minor role when filtering particles above 1µm.(22)

4.2 Filtration setup

The setup used for the filtration experiments consisted of a dead-end filtration unit, where a piston moves down through a cylinder at a constant pressure. Further information about the equipment is found in Appendix C. The filter is placed at the bottom of the cylinder, supported by a metal grid and the particle dispersion can then be placed in the cylinder, on top of the filter. Once the piston touches the liquid dispersion, the water is forced out through the filter, due to the pressure transferred from the piston, and the particles will be retained. The particles will deposit onto the filter and a filter cake is build.

To avoid leaking of the dispersion, the piston will have to fit tightly into the cylinder. This will generate some friction between the piston o-ring and the cylinder wall. To avoid errors in the results, the liquid pressure, at the point of contact between the piston and the liquid, will be measured and used in the subsequent calculations instead of the external pressure. Unfortunately, the regulation of the piston movement is still done in regard to external pressure, giving rise to a series of problems explained further in the presentation of the results.

In addition to the liquid and external pressures, the relative position, or length travelled, of the piston is measured as well. All the measured data is logged by an external on a PC, at a certain time interval specified by the user.

4.2.1 Method

Some of the original particle dispersions were diluted to a dry matter content of 10 and 5 g/L for the PMMA and PS particles respectively. The dry matter content of the original dispersion was determined gravimetrically, using small aluminum trays. The dilution was done with a 10 mM aqueous borax solution to maintain a pH value just above 9, as it will ensure, that all of the carboxylic acid groups on the PAA stabilizer are deprotonated, making the electrostatic repulsion amongst the individual chain (and particles) as high as possible. The conductivity of the diluted sample was also checked to ensure that they did not differ too much. As the highest and lowest conductivity of the samples was within a few percent, it was assumed that no regulation would be necessary.

Approximately 30 mL of the diluted dispersions were added to the cylinder fitted with a fresh filter and the piston was driven down, until it reached the liquid surface. The sampling rate was then set according to the assumed total length of filtration (to avoid too few or too many data points) and the filtration were started. The filtration was stopped when the piston reached the filter cake, as the consolidation of the filter cake is not a part of this work.

4.3 Presentation and discussion of the obtained results

Filtration experiments have been conducted on some of the synthesized batches. The term P_{liq} will be used for the pressure measured at the point of contact between the piston and the dispersion to be filtered and corresponds to the term P_e in the theory explained in section 4.1 and is as such not to be confused with P_l. The term P_{ext} will, however, be used here as the pressure measured, where the piston is connected to the rest of the filtration unit. If the pressure loss due to friction is termed P_{fric} then the following relation will exist: $P_{liq} = P_{ext} - P_{fric}$. All of the calculations of α will be done by using Eq. 4-11, with $\mu = 1 \cdot 10^{-3}\ Pa \cdot s$, $A = 3{,}95 \cdot 10^{-4}\ m^2$ and $P_e = \bar{P}_{liq}$, where $\bar{P}_{liq}$ is the average of all the measured values of P_{liq} within the linear section of the Ruth-plot. The dry matter content is given in kg/m^3, time in seconds, pressure in *Pa* and volume in m^3, making the units of α, m/kg.

4.3.1 Determination of α

For every successful filtration, a Ruth plot has been made, in order to determine the specific resistance, α, of the particular conditions used. As an example, a Ruth-plot from the filtration of PMMA-B is shown in Fig. 4.2. The slope, used to determine α from Eq. 4-11, is found by linear regression of the linear part of the Ruth-plot, marked in black. The pressure term in this equation are taken as the average P_{liq} over the data points included in the linear part of the Ruth-plot.

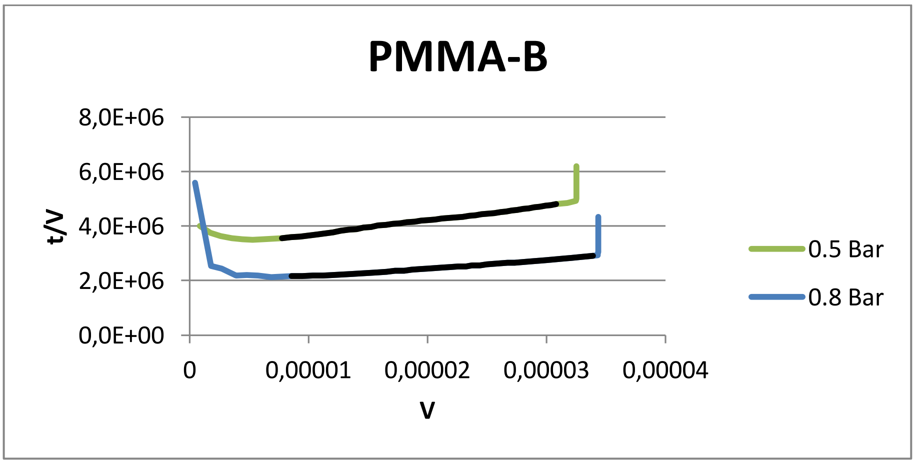

Fig. 4.2. Ruth-plot obtained from the filtration of PMMA-B at 0.5 and 0.8 bar

The determined values of α can be found in Table 4.1, as an average over the pressure range used for the filtration. As the Kozeny-Carman equation can be used to predict α from the size of the particles, and the porosity of the filter cake, a set of theoretically determined values is also found in Table 4.1. As the real porosity of the filter cake is unknown, it is assumed that the filter cake is composed of random close packed spheres, making $\varepsilon = 0{,}36$ (23).

Name	α_{exp}	$\alpha_{K\text{-}c}$
PMMA-B	7,05E+10	4,75E+10
PMMA-seeded	2,91E+10	1,33E+10
PS-co-P(PEGMA)	8,04E+13	1,06E+12
PS-C	2,17E+13	4,95E+11
PS-D	4,60E+12	4,15E+11

Table 4.1. Values of α obtained from dead end filtration experiments and the Kozeny-Carman equation, respectively

When comparing the obtained values of α, it is seen that all of the experimentally obtained α*'s* are larger than the ones from the Kozeny-Carman equation. Especially PS-C and PS-co-P(PEGMA) stands out, with a ratio between the two values of 43.8 and 75.9 respectively, while α_{exp} for PMMA-B and PMMA-seeded is only slightly larger than $\alpha_{K\text{-}c}$. All of the ratios are plotted in Fig. 4.3.

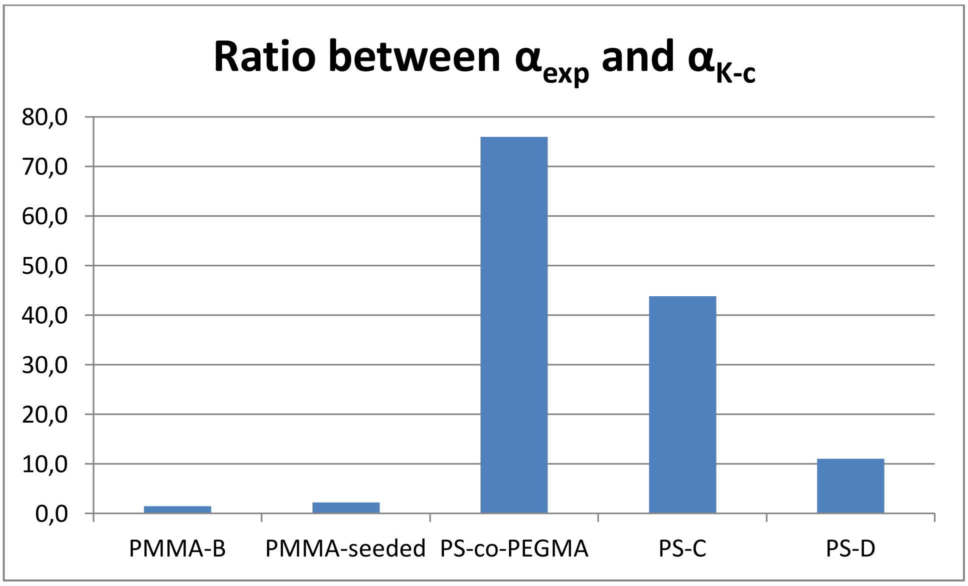

Fig. 4.3. Ratio between α_{exp} and $\alpha_{K\text{-}c}$

The reason for the higher α_{exp} of the PS particles is most probably due to the negatively charged PAA surrounding the particles, as the Kozeny-Carman equation is only valid when there are no electrochemical interactions between the particles and the liquid (24). In addition to this, the dual-layer morphology of the PS-co-P(PEGMA) particles seems to have an effect to. It is however not clear what causes the difference between PS-C and PS-D as they are approximately the same size. The only known difference between the two is the charge density, but since the charge density of PS-D, seemingly, is larger than that of PS-C, this cannot account for the difference in the measured values of α. The measured charge density is however debatable, as mentioned in section 3.9, making the comparison between charge density and α_{exp} unsustainable.

4.3.2 Limitations of the method used

As mentioned in section 4.2, the movement of the piston will cause friction between the piston and the cylinder wall. This friction puts a limit to the usable pressure range, as the external pressure will have to be high enough to overcome it. Additionally, the amount of friction is not constant through the length of the cylinder, so the liquid pressure will vary as a function of piston position, even though the external pressure is constant. The lower pressure limit was found to be 0.5 bars, but even still, some of the results, from runs at this pressure, would have to be discarded. This was either due to the filtration stopping too soon, as the friction exceeded the external pressure, or to very large fluctuations in the liquid pressure. The latter was the more common of the two and could actually happen at higher pressures as well, although not as often. Fig. 4.4 and Fig. 4.5 are examples of this, showing the external and liquid pressure as function of piston position, with the fist being the typical result of runs below 0.5 bars.

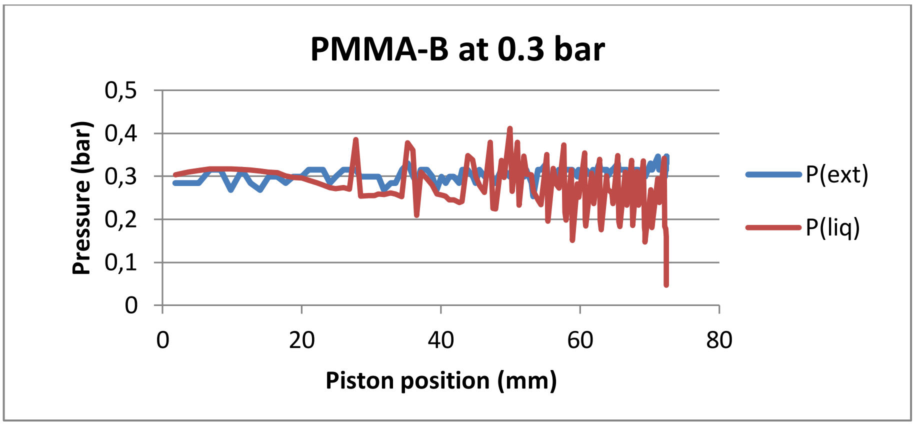

Fig. 4.4 P_{ext} and P_{liq} measured as a function of piston position for the filtration of PMMA-B at 0.3 bar

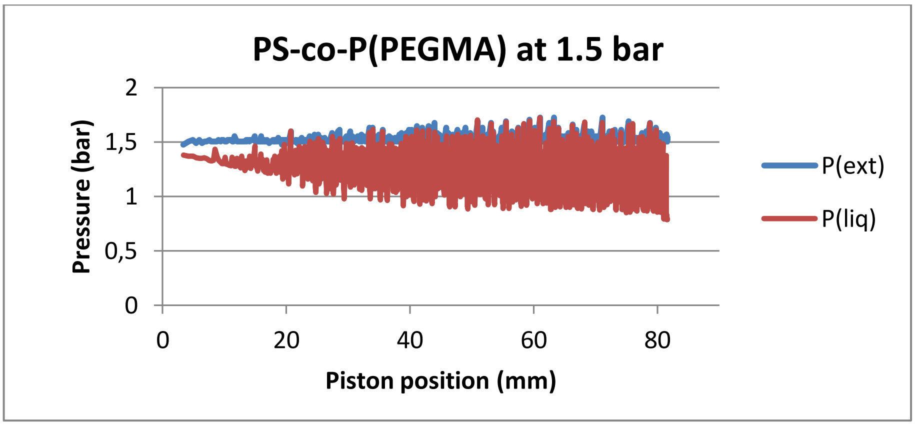

Fig. 4.5. P_{ext} and P_{liq} measured as a function of piston position for the filtration of PS-co-P(PEGMA) at 1.5 bar

For most of the runs where P_{liq} fluctuates, the determined value of α appeared to be significantly larger than for runs where P_{liq} didn't fluctuate as much. The Ruth-plot would also be less linear and in the worst cases have a jagged appearance. An example of this is shown in Fig. 4.6 and is taken from the same run as Fig. 4.3. The linear trend line is added only to illustrate the non-linearity of the Ruth-plot.

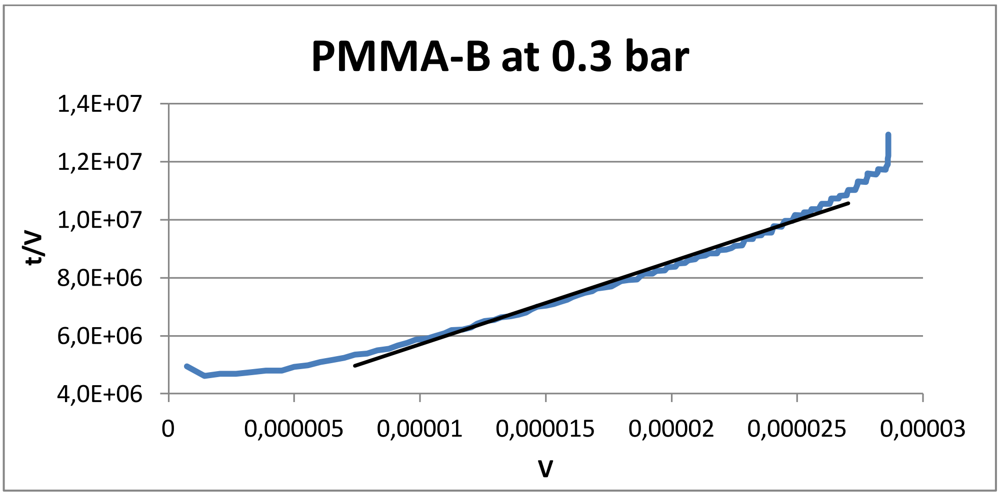

Fig. 4.6. Ruth-plot from the filtration of PMMA-B at 0.3 bar, showing the effect of a fluctuating P_{liq}

As mentioned, the friction varies down through the cylinder, also for the runs where the above mentioned phenomenon does not occur, with Fig. 4.7 being an excellent example of this. The shape of the P_{liq} curve and the amount of pressure lost to friction, varies greatly between the different runs and seems to be affected, amongst other things, by the way the piston is inserted into the piston-holder.

The lower pressure limit is particularly a problem for the PMMA particles, where α is small. The low resistance to filtration makes it impossible for the filtration unit to move the piston fast enough to keep the external pressure constant. This leaves a very small usable pressure range, making it difficult to obtain reliable data from runs at different pressures. The only ways to overcome this is to; either increase the dry matter content, lowering the number of runs which are possible from one batch; or change the regulation mechanism on the filtration unit in such a way, that the regulation is done on basis of the liquid pressure instead of the external pressure.

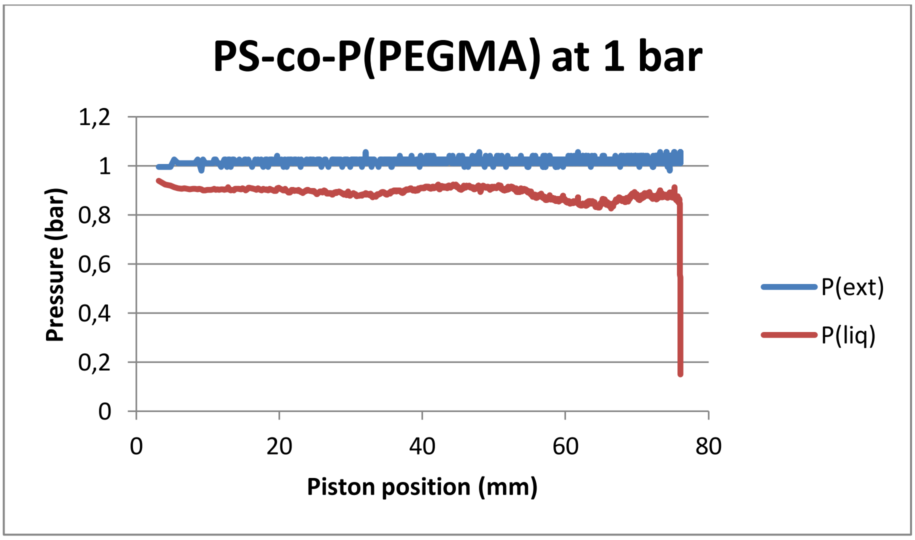

Fig. 4.7. P_{ext} and P_{liq} measured as a function of piston position for the filtration of PS-co-P(PEGMA) at 1 bar

On top of the problems arising from friction, it was, as most of the filtration runs were finished, found that the piston was slightly crocked, due to a bend in the piston holder. This meant that one side of the cylinder casing would be lifted by the force from the piston to maintain the cylinder wall and the piston parallel. It was also found, that one of the large screws, responsible for the movement of the piston, were crocked as well, making the piston wiggle a bit from side to side, when moving up and down. It is not clear to what extend this have affected the filtration experiments and for how long it has been a problem

4.3.3 Pressure dependency of α

For incompressible material, α is considered independent of pressure, as is the case in the theory in section 4.1. This is however not always the case, and the pressure dependency of α, for a filter cake consisting of the synthesized particles, was attempted examined. The problems with the equipment and the lower pressure limit, mentioned in section 4.3.2, would, however, prove this to be difficult, as a decent set of data, from filtration of the same dispersion at different pressures, were hard to obtain.

Fig. 4.8 shows the determined values of α at the different pressures used, note the logarithmic scale of α. Even though there are only two useable data sets from each batch, α does not appear to be pressure dependent within the ranges used here. There is, however, one exception; PS-co-P(PEGMA). When going from 0.5 to 1 bar, there is a slight increase in α of 17%, while it is 49% when going from 1 to 1.5 bar. It can however be debated if the value at 1.5 bar is valid, as P_{liq} did fluctuate a lot during this run, hence the bracket. The reason why it is still presented is that the Ruth-plot for this run, shown in Fig. 4.9, does not have the same issues as the other runs with a fluctuating P_{liq}, as it is very linear and non-jagged.

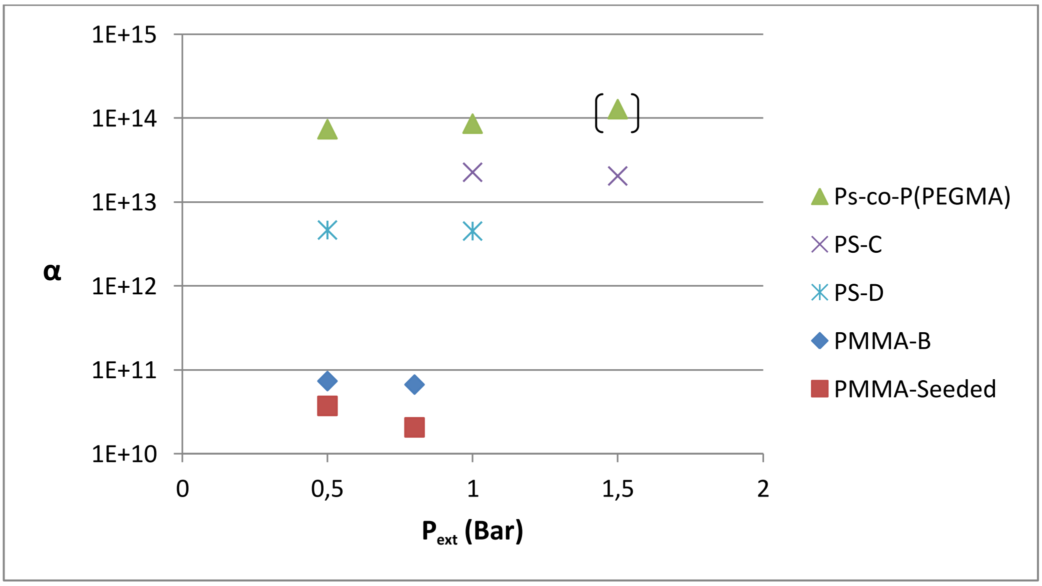

Fig. 4.8. Experimentally determined values of α at different pressures, note the logarithmic scale

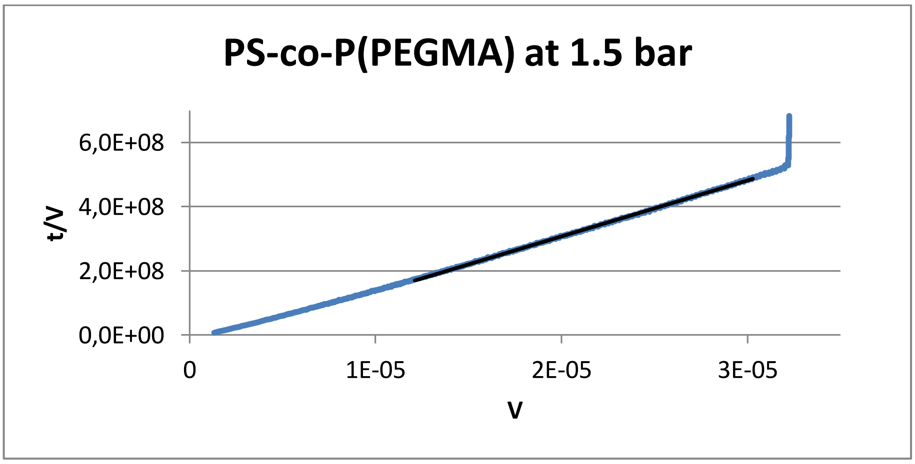

Fig. 4.9. Ruth-plot from the filtration of PS-co-P(PEGMA) at 1.5 bar

It could also be discussed whether the increase is significant in regards to the flux. This can possibly be determined by inserting the values of α for the PS-co-P(PEGMA) into Eq. 4-7Eq. 4-8 and then use Eq. 4-7 to simulate the changes in flux, with the changes in α and pressure.

Fig. 4.10 shows such a simulation, where the filtrate volume has been set to 30 mL, and includes both one with and one without the data from the 1.5 bar run. The plotted points are from the lowest and highest couple of α and P_{liq}, as well as from the average of the two. From this it seems, that the measured change in α is only significant if data from the 1.5 bar run is included. This can indicate one of two things. Either are the 1.5 bar data valid and a filter cake composed of these particles seems to be somewhat compressible, with a critical pressure above 1.5 bar, or the data are not valid and the filter cake are not compressible at this pressure range.

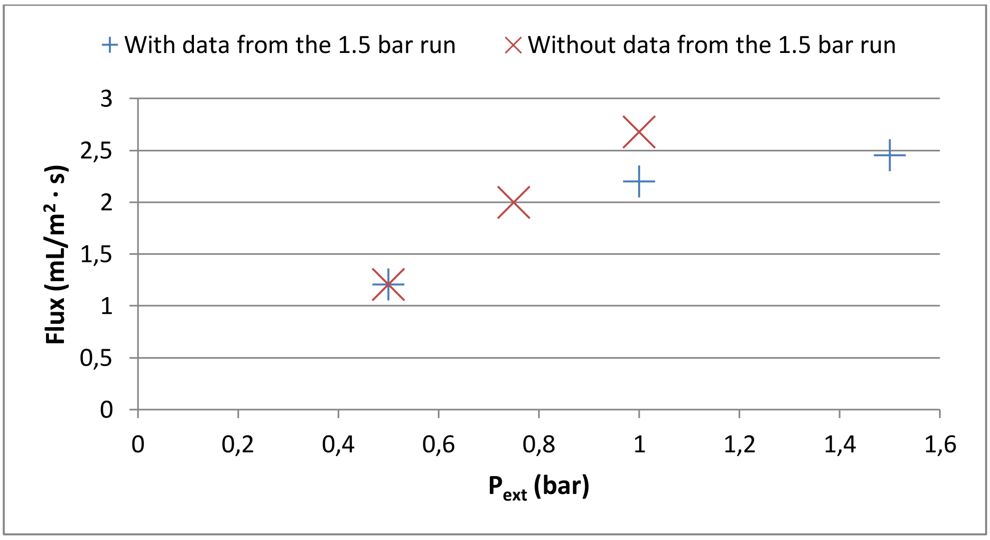

Fig. 4.10. Simulation of the flux made from α_{exp}

Some additional filtration experiments with PS-co-P(PEGMA) were conducted, with the external pressure ranging from 0.5 to 2 bar. The results are shown in Fig. 4.11 and here, no significant change in α was found at the different pressures. It should be noted, that only approximately 9 mL of dispersion were filtered here, while approximately 30 mL were used in the first filtration experiment. As the values of α found the second time are also generally smaller than the first, this difference in filtrate volume might have an, as of now, unknown effect on the specific resistance of the filter cake. It might be possible that some creep can occur over time (it takes more than 4½ hours to filter 30 mL at 1 bar whereas it takes less than 30 minutes to filter 9 mL at 1 bar), but this is only speculative.

If it is assumed that half of the added PEGMA have ended up on the particle surface, The PEG subunit density can be calculated to be 0.67 mmol/m^2, which can be compared to the charge density of 0.042 mEq/m^2. As PEG's in water can produce a very high osmotic pressure(25), the dual layer morphology of these particles will cause a higher osmotic pressure in the filter cake, which might help explain the found pressure dependency, if any(22).

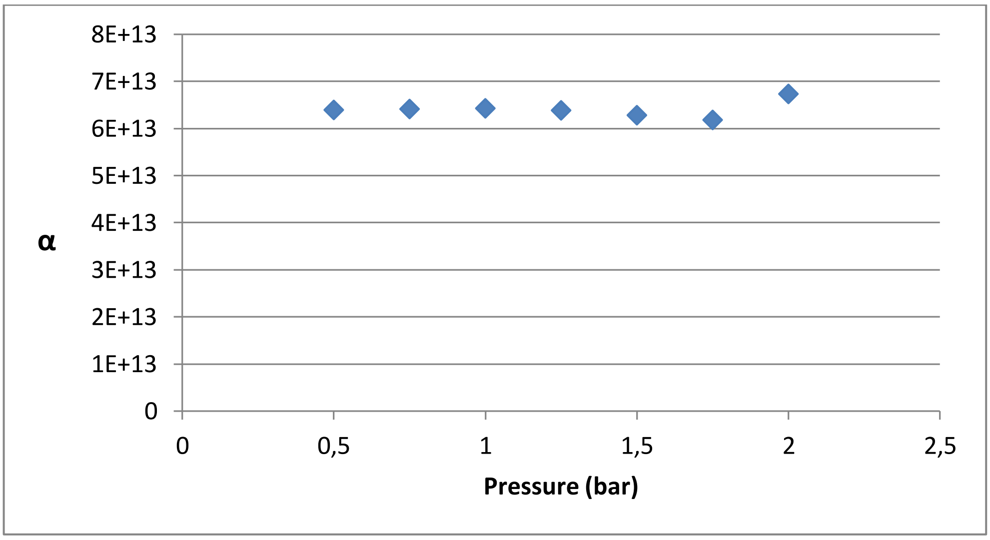

Fig. 4.11. α obtained from a new set of filtrations of PS-co-P(PEGMA) at 0.5 to 2 bar

4.3.4 Blinding effects

To investigate how a combination of particles with different sizes would behave during filtration, a series of runs were made using a mixture of PS-co-P(PEGMA) and PMMA-B (small/medium) or of PS-co-P(PEGMA) and PMMA-seeded (small/large). The diluted dispersion from before were mixed in a 1:1 vol. ratio, to a final dry matter content of 7.5 g/L. The results from this are shown in Fig. 4.12, with several important elements to notice.

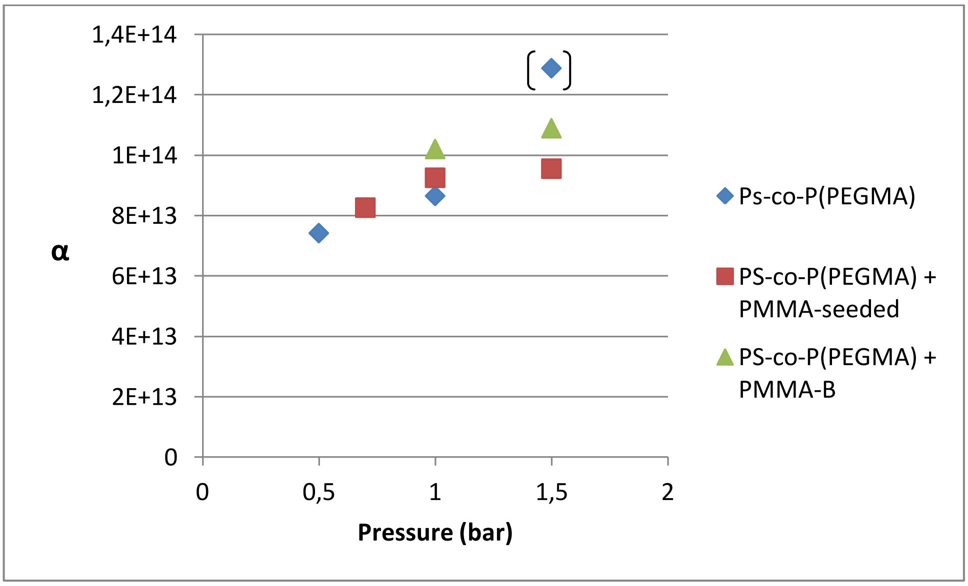

Fig. 4.12. α from filtration of 1:1 vol. mixtures of dispersions with large an small particles

Firstly, the resistance of the filter cake seems to be governed mostly be the small particles, as the values of α are close to, but higher than, the ones obtained from filtration of PS-co-P(PEGMA) alone, indicating that some sort of blinding effect is taking place. This is backed up by the difference in α between the two mixtures, as it is more than 200 times larger than the difference between the filtration of PMMA-B and PMMA seeded alone. Furthermore, it looks like the small/medium combination will give the highest resistance of the two mixtures, probably due to more efficient blinding by the small particles taking up the voids in the packed medium particles. This is illustrated in Fig. 4.13, where circles, with the correct ratios, are representing the particles used.

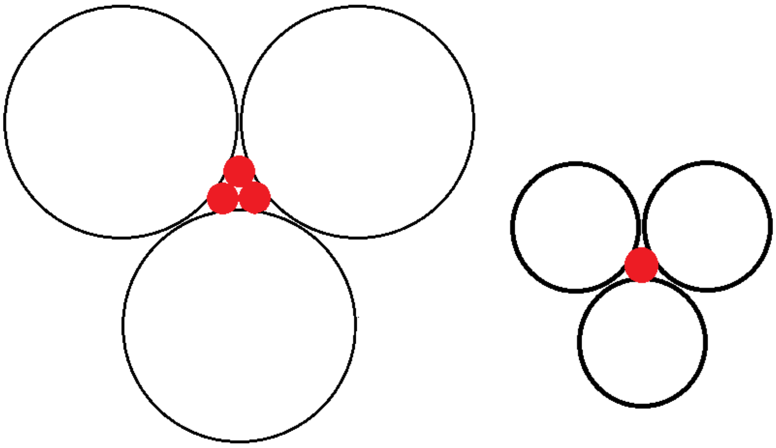

Fig. 4.13. Illustration of large (12 µm) and medium (6.5 µm) particles with small (1.5 µm) particles blinding the voids created between the large/medium particles

It is, however, important to keep in mind, that even though the larger particles will have the highest weight fraction (from the 1:1 vol. mixture of dispersion with 10 and 5 g/L for the larger and smaller particles respectively), they will be greatly outnumbered by the smaller ones. A different result might appear if the particles were to be mixed 1:1 in numbers.

Secondly, All of the measured values of α increases with increasing pressure, just as it was found for the PS-co-P(PEGMA) particles alone. This supports the notion, that a filter cake composed of this type of particles, either alone or combined with others, might be slightly compressible. The value from the 1.5 bar filtration run of PS-P(PEGMA) is higher than the one from PS-P(PEGMA) + PMMA-B at the same pressure, even though the reverse is true for the values at lower pressures. The notion of this run not being valid is thus strengthened, but the real value might still be higher than the one at 1 bar.

5 Conclusion

Several batches of particles have been synthesized using dispersion polymerization techniques, covering the following three different types:

- Poly(methyl methacrylate) (PMMA) particles with a non-ionic grafted stabilizer made from Polyvinylpyrrolidone (PVP)
- Polystyrene (PS) particles with an anionic grafted stabilizer made from Poly(acrylic acid) (PAA)
- Polystyrene particles (PS) with a dual layer morphology of the shell made from grafted Poly(acrylic acid) (PAA) and directly co-polymerized Poly(ethylene glycol)-methacrylate (PEGMA)

All of the synthesized particles fulfill most of the requirements outlined in the aim presented in section 2, with the following exceptions.

Particles with a water swellable core were not synthesized although methacrylic acid was added as co-monomer with the expectation that it would be incorporated into the particles. This did, however, not happen, probably due to interactions between PVP and MAA. Experiments indicate that the MAA will make some of the PVP unavailable for grafting, reducing the stabilizing potential while keeping the MAA-PVP couple in solution. As the PS particles were synthesized with PAA as stabilizer instead of PVP, MAA might co-polymerize with styrene and be incorporated into the particles, although this have not been attempted.

All of the PS particles are negatively charged, because of the grafted PAA used as stabilizer. This method of introducing charges will, however, also limit the ability to independently vary size and charge density, as particle size is strongly linked to the amount of available stabilizer. Furthermore, the charge density measured by pH-titration is somewhat debatable due to coagulation of the particles at low pH.

The size range covered is approximately 1.5 to 12.5 µm, while the monodispersity, measured as the geometric standard deviation (GSD), varies from approximately 1.2 to 2.4 with the PS particles generally having the lowest GSD. Theory on size control and the ability to produce monodisperse particles have been found and presented from literature studies, which show that stabilization and locus of polymerization both play important roles. This knowledge have been used in the slightly different PS-co-P(PEGMA) particles.

Some of the synthesized particles were used in dead end dewatering filtration experiments, with the aim of measuring the specific resistance of the filter cake, α. This value was then compared to predictions of α from the Kozeny-Carman equation, based on the particle size. It was found that the filter cake resistance of the PMMA particles was very close to the predicted value, while the resistance of the PS particles all was higher than predicted. Especially the particles made with both PAA and PEGMA as stabilizer showed this tendency, with the measured α being more than 75 times higher than the predicted value.

During the filtration experiments, runs were made at different pressures to investigate the compressibility of the formed filter cakes. Only the PS-co-P(PEGMA) particles showed an increase in α with increasing pressure, and only if the amount filtered were high enough to allow the entire run to last several hours.

Finally, blinding effects, when using a mixture of different sized particles, were investigated. This showed, that the filter cake resistance is mainly governed by the smaller particles, as the values of α were in the same range as those for PS-co-P(PEGMA) alone. Besides this, the blinding effect were more pronounced when combining small (1.5 µm) and medium (6.5 µm) particles in contrast to small (1.5 µm) and large (12 µm). The results from the blinding experiments supported the ones from the longer filtration runs of PS-co-P(PEGMA), with α increasing with increasing pressure

All in all, the route taken to synthesize the PS-co-P(PEGMA) particles seems to be the most viable for now. These particles were the ones closest to what are needed, mimicking some of the behavior seen when employing membrane filtration to waste water containing organic particles. If combined with co-polymerization of anionic monomers such as (meth)acrylic acid or if a method can be found to control particle size and charge density independently, then this type of particles would be very interesting, when regarding organic model colloids in the µm range.

As an end note, several problems with the filtration equipment were discovered during the filtration experiments and it is unknown whether this has affected the obtained result in any way not taken into account in the presentation and discussion of the dewatering filtration results.

Appendix A Nomenclature

Symbol/ abbreviation	Description
MBR	Membrane Bio Reactor
EPS	Extra cellular polymeric substances
MW	Molar weight
PEG	Poly(ethylene glycol)
PVP	Polyvinylpyrrolidone
PAA	Poly(acrylic acid)
α-carbon	The carbon atom next to a functional group
α-hydrogen	Hydrogen atom(s) attached to the α-carbon
MMA	methyl methacrylate
PMMA	Poly(methyl methacrylate)
PVP-g-PMMA	The graft co-polymer produced from chain transfer to PVP in the presence of MMA
MAA	Methacrylic acid
NaMA	Sodium methacrylate
PS	Polystyrene
AIBN	Azobisisobutyronitrile
MeOH	Methanol
EtOH	Ethanol
PEGMA	Poly(ethylene glycol) methacrylate
PP	Polypropylene
SEM	Scanning electron microscopy
Q_{min}	The minimum amount of grafted stabilizer needed to prevent large particle coalescence
Q_{max}	The maximum amount of grafted stabilizer allowed to prevent secondary particle formation
a	Material dependent proportionality constant when calculation r_g
b	Material dependent exponential constant when calculation r_g
A_p	Particle area
V_p	Particle volume
x	Degree of conversion from monomer to polymer
d_{50}	Average particle diameter
GSD	Geometric standard deviation
r_g	Radius of gyration
Eq.	Equivalent
s	Dry matter content
A_{spec}	Weight specific area
V	Volume
J	Flux
μ	Dynamic viscosity
R	Specific resistance
α	Specific resistance to filtration when using material coordinates
P_l	Liquid pressure in the filter cake
P_s	Solid pressure in the filter cake
L and l	Length/height of the filter cake

P_e	External pressure
P_{liq}	The pressure measured between the piston and the filtrate (=P_e)
Symbol/ abbreviation	Description
P_{fric}	Pressure loss due to friction
P_{app}	Applied pressure (P_{app}=P_{liq}+P_{fric})
ε	Porosity
S_0	Volume specific area
A	Cylinder cross sectional area (membrane area)
r_p	Pore radius
V_f	Cumulative filtrate volume
ρ_p	Particle density
ω	Amount of material deposited pr m^2
t	Time
α_{exp}	α determined experimentally
α_{K-c}	α determined from the Kozeny-Carman equation

Appendix B List of chemicals

Chemical	Cas nr.	Purchased from	Purity	Additional info
Methyl methacrylate	80-62-6	Sigma-Aldrich	99 %	Contains 30 ppm monomethylether hydroquinone
Methacrylic acid	79-41-4	Sigma-Aldrich	99 %	
Sodium methacrylate	5536-61-8	Sigma-Aldrich	n/a	
PVP-K30	9003-39-8	Sigma-Aldrich	n/a	60 kDa
AIBN	78-67-1	Sigma-Aldrich	98 %	Recrystallized before use
Methanol	67-56-1	Sigma-Aldrich	99.8 %	
Ethanol	64-17-5	Kemetyl	99.9 %	
Styrene	100-42-5	Sigma-Aldrich	99 %	Contains 10-15 ppm 4-tert-butylcatechol
Poly(acrylic acid)	9003-01-4	Sigma-Aldrich	35 % in H_2O	100 kDa
Poly(acrylic acid)	9003-01-4	Wako	n/a	25 kDa
NaOH	1310-73-2	J. T. Baker	50 % in H_2O	
$NaClO_4$	7601-89-0	Merck	n/a	Monohydrate
$HClO_4$	7601-90-3	Merck	n/a	
PEG monomethyl ether	9004-74-4	Sigma-Aldrich	n/a	5 kDa
Methacrylic anhydride	760-93-0	Sigma-Aldrich	94 %	Contains 2000 ppm Topanol A
Pyridine	110-86-1	Fisher Scientific	n/a	Anhydrous
DMAP	1122-58-3	Sigma-Aldrich	n/a	
Dichloromethane	75-09-2	Sigma-Aldrich	n/a	
Diethyl ether	60-29-7	Sigma-Aldrich	99.5 %	
Borax (sodium tetraborate)	1330-43-4	n/a	n/a	decahydrate
Hydroquinone	123-31-9	Acros Organics	99 %	

Appendix C Equipment information

pH titrations:

The titrations were performed by the use of two *ABU901 Autoburettes*, combined with a *SAM90 Sample station* and a *Titralab TIM900 Titration manager*, all from *Radiometer – Copenhagen*. The PC program used to control the titrations and collect the data was *TimTalk 9* from *LabSoft*.

Size measurements:

The particle sizes were measured from multiangle light scattering by the use of a *Microtrac II – particle size analyser* and a *Recirculator*, both from *Leeds & Northrup*. Before measurements the equipment was set to automatically give the 16 and 84 percentile values used in the calculations of GSD as well as the d_{50} value presented as average particle diameter.

Filtration:

The dead end filtration unit used in this work is shown in Fig. C.1, with the cylinder and piston in the middle. The filters used were *Durapore membrane filters, 0.22 µm GV from Milipore* and the piston o-ring were lubricated with a medium density, high vacuum, silicon grease.

Fig. C.1. The dead end filtration unit used in this work

Appendix D Bibliography

1. **Baker, Richard W.** *Membrane technology and applications.* s.l. : John Wiley & Sons Ldt., 2004.

2. **Hinge, Mogens.** *Synthesis of soft shell poly(styrene) colloids for filtration experiments.* Section of Chemistry, Aalborg University. 2006. Ph.D. dissertation.

3. **Stephenson, Tom, et al.** *Membrane Bioreactors for Wastewater Treatment.* s.l. : IWA publishing, 2000.

4. **Keiding, Kristian.** *Phenomenologies in Physical Chemistry.* 2009. No other informations availible .

5. **Arshady, R.** Suspension, emulsion, and dispersion polymerization: A methodological survey. *Colloid & Polymer Science.* 1992, 270, s. 717-732.

6. *Suspension polymerisation of methyl methacrylate using sodium polymethacrylate as a suspending agent.* **Georgiadou, Styliani og Brooks, Brian W.** s.l. : Elsevier, 2005, Chemical Engineering Science, Årg. 60, s. 7137–7152.

7. **Gilbert, G. Robert og Thickett, Stuart C.** Emulsion polymerization: State of the art in kinetics and mechanisms. *Polymer.* 2007, 48, s. 6965-6991.

8. **Hinge, Mogens og Keiding, Kristian.** Systematical investigation of the synthesis of core-shell poly(styrene-co-acrylic acid) colloids with varying shell thickness and core diameter. 2006.

9. **Kun, Cao, Bo-Geng, Li og Zu-Ren, Pan.** micron-size functiona uniform PMMA particles by dispersion copolymerization in polar media. *Macromolecular Symposium.* 2000, 150, s. 195-200.

10. **Paine, A. J.** Dispersion polymerization of styrene in polar solvents. 7. A simple mechanistic model to predict particle size. *Macromolecules.* 23, 1990, s. 3109-3117.

11. **de Hoog, Elisabeth Hendrika Andrea.** *Interfaces and crystallization in Colloid-Polymer suspensions.* s.l. : Proefschrift Universiteit Utrecht, 2001. Dissetation.

12. **Kawaguchi, Seigou og Ito, Koichi.** Dispersion polymerization. *Adv Polym Sci.* 2005, 175, s. 299-328.

13. **Tseng, C. M., et al.** Uniform Polymer Particles by Dispersion Polymerization in Alcohol. *Journal of Polymer Science, Part A: Polymer Chemistry Edition.* 1986, 24, s. 2995-3007.

14. **Shen, S., Sudol, E. D. og El-Aasser, M. S.** Dispersion polymerization of methyl methacrylate: Mechanism of particle formation. *Journal of polymer science, Part A: polymer chemistry.* 32, s. 1087-1100.

15. **Paine, Anthony James, Luymes, Wayne og McNulty, James.** Dispersion Polymerization of Styrene in Polar Solvents. Influence of Reaction Parameters on Particle Size and Molecular

Weight in Poly(N-vinylpyrrolidone)-Stabilized Reactions. *macromolecules.* 1990, 23, s. 3104-3109.

16. **Stevens, Malcolm P.** *Polymer Chemistry - An Introduction.* s.l. : Oxford University Press, 1999.

17. **Shen, S., Sudol, E. D. og El-Aasser, M. S.** Control of particle size in dispersion polymerization of methyl methacrylate. *Journal of polymer science - Part A: polymer chemistry.* 31, 1993, s. 1393-1402.

18. *Solution properties and unperturbed dimensions of poly(vinylpyrrolidone).* **Ali, Sabz og Ahmad, Noor.** 3, s.l. : Wiley, British Polymer Journal, Årg. 14, s. 113-116.

19. *Protecting Polymers in Suspension of Metal Nanoparticles.* **Hirai, Hidefumi og Yykura, Noboru.** s.l. : John Wiley & Sons Ltd., Polymers for Advanced Technologies, Årg. 12, s. 724-733.

20. *Reactive Surfactants in Emulsion Polymerization.* **Guyot, A. og Tauer, K.** s.l. : Spinger, Advances in Polymer Science, Årg. 111, s. 44-65.

21. *Pressure and concentration profiles in filter cake consisting of core/shell latex particle.* **Christensen, Morten Lykkegaard, et al.** s.l. : Elsevier, 2006, Colloids and Surfaces A, Årg. 290, s. 295-303.

22. *Osmotic effects in sludge dewatering.* **Keiding, Kristian og Rasmussen, Michael R.** s.l. : Elsevier, 2003, Advances in Environmental Research, Årg. 7, s. 641-645.

23. **Song, Chaoming, Wang, Ping og Makse, Hernán A.** A phase diagram for jammed matter. *Nature.* 2008, Årg. 454, s. 629-632.

24. **Carrier, David W.** Goodbye, Hazen; Hello, Kozeny-Carman. 2003, s. 1054-1056.

25. *Osmotic Pressure of Aqueous Polyethylene Glycols.* **Money, Nicholas P.** 1989, Plant Physiology, Årg. 91, s. 766-769.